JNC TN9400 2001-084

Interpretation of the CABRI-RAFT RB1 and RB2 Tests through Detailed Data Evaluation and PAPAS-2S Code Analysis

August 2001

O-arai Engineering Center
Japan Nuclear Cycle Development Institute

Ⓢ

JNC TN9400 2001-084
August, 2001

Interpretation of the CABRI-RAFT RB1 and RB2 tests through detailed data evaluation and PAPAS-2S code analysis

Yoshitaka FUKANO※ and Ikken SATO※

Abstract

The CABRI-RAFT RB1 and RB2 tests were aiming at a study on impact of fuel pin failure under an overpower condition leading to fuel melting. Using a special technique, combination of through-cladding failure and fuel melting was realized. In the RB1 test, fuel ejection was prevented under a limited fuel melting condition. On the other hand, significant fuel melting was applied in the RB2 test so as to get the fuel ejection, thereby obtaining information on the fuel ejection behavior.

Interpretation for these tests through the detailed experimental data evaluation and the PAPAS-2S code analysis is performed in this study. Through this study, it is indicated that molten fuel ejection can be prevented with the low smear density fuel as far as the fuel melting is not large for a slit-type cladding defect. Fuel ejection becomes possible in the case of significant fuel melting with a very thin solid fuel shell surrounding the molten fuel cavity. However, the rapidness of the fuel ejection with the low smear density fuel is less pronounced compared with that of the high smear density fuel.

It is also confirmed that there is considerable DN-precursor release into the coolant flow already before fuel ejection. This result is very useful for evaluation of anomaly detection with DN signal observation.

※Nuclear System Safety Research Group, Advanced Technology Division, O-arai Engineering Center

JNC TN9400 2001-084
2001年8月

試験データの詳細分析及びPAPAS-2Sコード解析による
CABRI-RAFT計画RB1，RB2試験結果の解釈
(研究報告書)

深野 義隆※ 佐藤 一憲※

要旨

CABRI-RAFT計画のRB1及びRB2試験は燃料溶融に至る過出力条件における、ピン破損の影響を解明することを目的としている。これらの試験では、特殊な技術を用いて燃料溶融と被覆管の貫通破損を実現した。RB1試験では、少量の燃料溶融条件下での溶融燃料放出の抑制を確認するとともに、一方のRB2試験では、溶融燃料放出挙動に関する情報を得るため、大量の燃料溶融条件とした。

本研究では、RB1,RB2試験データの詳細な分析及びPAPAS-2Sコードによる解析評価を実施し、これらに基づいて試験結果の解釈を行った。本研究を通じて、低スミア密度燃料では、スリット型の被覆管破損を想定しても軽微な燃料溶融の範囲では、溶融燃料の放出は抑制されることが示された。一方、大量の燃料溶融により、溶融キャビティ外側の固相燃料殻の薄い条件では、溶融燃料の放出を生じ得ることも明らかにした。しかしながら、低スミア密度燃料では、高スミア密度燃料と比較すると溶融燃料の放出速度も緩慢となることがわかった。

また、両試験では、溶融燃料の放出前に、既にかなりのDN先行核が冷却材流路中へ移行しており、これは、DN信号による異常検知性を評価する上で有効なデータである。

※大洗工学センター 要素技術開発部 リスク評価研究グループ

Contents

Page
Abstract ---------- i
要旨 ---------- ii
Contents ---------- iii
List of Table and Figures ---------- iv
1. Introduction ---------- 1
2. Overview of the RB1 and RB2 tests ---------- 2
  2 - 1. Fuel characteristics ---------- 2
  2 - 2. Test conditions ---------- 2
  2 - 3. Summary of the test results ---------- 2
3. PAPAS-2S analysis for the RB1 and RB2 tests ---------- 4
  3 - 1. Fuel-to-cladding gap conductance model ---------- 4
  3 - 2. Analysis for the RB1 test ---------- 4
  3 - 3. Analysis for the RB2 test ---------- 5
4. Interpretation of the test results based on the experimental data analysis ---------- 7
  4 - 1. Interpretation of the RB1 test ---------- 7
  4 - 2. Interpretation of the RB2 test ---------- 8
5. Discussion ---------- 11
6. Conclusions ---------- 13

List of Table and Figures

Table 1 SCARABIX-CABRI type fuel characteristics ------------------------------ 14

Figure 1 Simplified drawing of the notch in the RB1 and RB2 tests ---------- 15
Figure 2 Power and flow history in the RB1 and RB2 tests -------------------- 16
Figure 3 Radial cut of the RB1 test pin at 40cm from BFC -------------------- 17
Figure 4 Radial cut of the RB1 test pin at 46cm from BFC -------------------- 18
Figure 5 Axial cut of the RB1 test pin from 51.45 to 54.95 cm from BFC -------- 19
Figure 6 Fractional melting radius in the FAST and RAFT slow-TOP tests ----- 20
Figure 7 Average enthalpy at PPN in the FAST and RAFT slow-TOP tests ---- 21
Figure 8 Axial power profile of the RB1 test fuel ------------------------------ 22
Figure 9 Power history of the RB1 test used in the PAPAS-2S analysis -------- 23
Figure 10 Coolant flow history of the RB1 test
used in the PAPAS-2S analysis -------------------- 24
Figure 11 Comparison of coolant temperature profile
at steady state in the RB1 test -------------------- 25
Figure 12 Comparison of coolant temperature history
at TFC in the RB1 test -------------------- 26
Figure 13 Comparison of fuel melting boundary in the RB1 test ---------- 27
Figure 14 ^{137}Cs axial profile before and after the RB1 test -------------------- 28
Figure 15 Power history of the RB2 test used in the PAPAS-2S analysis ------- 29
Figure 16 Comparison of coolant temperature profile
at steady state in the RB2 test -------------------- 30
Figure 17 Comparison of coolant temperature history
at TFC in the RB2 test -------------------- 31
Figure 18 Comparison of fuel melting boundary in the RB2 test ---------- 32
Figure 19 DN signal in the RB1 test -- 33
Figure 20 Inlet and outlet flow history in the RB1 test ------------------------------ 34
Figure 21 ^{106}Ru axial profile before and after the RB1 test -------------------- 35
Figure 22 Inlet and outlet flow history after the SCARM in the RB1 test---------- 36
Figure 23 Inlet and outlet flow history
during the power ramp in the RB2 test ----------------------------- 37
Figure 24 DN signal in the RB2 test -- 38

Figure 25 Inlet and outlet flow history during LOF in the RB2 test ---------- 39

Figure 26 Microphone signal in the RB2 test -- 40

Figure 27 Inlet and outlet pressure in the RB2 test ------------------------------- 41

Figure 28 Voiding zone extension after the molten fuel ejection in the RB2 test -------------------- 42

Figure 29 Neutron hodoscope data during LOF in the RB2 test ---------- 43

Figure 30 Comparison of RB2 voiding zone extension with the other CABRI tests -------------------- 44

Figure 31 Coolant temperature history from 30 to 75 cm from BFC in the RB2 test -------------------- 45

Figure 32 Destructive and non-destructive PIE results in the RB2 test ---------- 46

Figure 33 Axial cut of the RB2 test pin from 48.6 to 52.44 cm from BFC ------- 47

Figure 34 Void detector signal in the RB2 test ------------------------------- 48

Figure 35 Fuel ejection and void development behavior in the RB2 test ------- 49

Figure 36 Displacement transducer signal in the RB2 test -------------------- 50

Figure 37 Axial profile of ^{60}Co gamma scanning in the RB2 test ---------- 51

Figure 38 Radial cut of the RB2 test pin at 38.6 cm from BFC -------------------- 52

Figure 39 Coolant temperature history during the LOF in the RB2 test ---------- 53

Figure 40 Summary of the TREAT/J1 and R12 tests ------------------------------ 54

1. Introduction

The RB1 and RB2 tests in the CABRI-RAFT program (from 1996 to 2001) were performed under the collaboration between IPSN and JNC. In these tests, impact of fuel pin failure under an overpower condition leading to fuel melting was studied. Using pre-defected fuel pins, a slow TOP transient corresponding to a control-rod withdrawal-type incident was applied.

Through the study in the CABRI-FAST program, it was clarified that the low smear density fuel has a very high failure threshold. Most fuel pins will not fail under the slow-TOP type overpower condition except for an extremely high overpower condition which is clearly beyond the scope of the RB series tests discussed here. However, considering the statistic variation of the numerous fuel pins in the core, failure of a few fuel pins cannot be ruled out. In order to simulate consequence of pin failure under such condition, special pre-defected pins were used in these tests.

The RB1 and RB2 tests resulted in no fuel ejection and significant fuel ejection, respectively. The RB1 test provided useful information to consider the threshold for fuel ejection, while the RB2 test brought valuable information on fuel ejection behavior which is important for consideration of coolability after fuel ejection.

In this study, detailed examination of experimental results was performed with a help of PAPAS-2S analysis which provided precise information on fuel thermal conditions.

2. Overview of the RB1 and RB2 tests

2-1. Fuel characteristics

The SCARABIX-CABRI type fuel pins whose main characteristics are presented in Table 1, were used in the RB1 and RB2 tests which have large diameter and annular pellet design, and were pre-irradiated up to approximately 7 at.% in the Phenix reactor. These fuel pins were also used in the slow-TOP tests in the CABRI-FAST program such as PFX, PF1 and MF2, and showed non-failure result even at the maximum fuel linear power rating of 1248W/cm in the MF2 test.

In order to realize pin failure, RB1 and RB2 pins had through-clad slits filled with a fusible metal at 40 cm and 48cm from BFC (bottom of fissile column), respectively, as depicted in Figure 1.

2-2. Test conditions

In the RB1 test, power was increased from the initial linear power rating of 401 W/cm up to 850 W/cm with the ramp rate of 0.63 %Po/s as presented in Figure 2. After reaching the maximum power, LOF was initiated with the constant power so as to realize a cladding failure. This power level was selected in order to guarantee minimum fuel melting within the uncertainty and to prevent excessive fuel melting.

After the power plateau, LOF was applied leading to 40% of the initial flow rate so as to increase the fusible metal temperature. Then flow was increased again to 70% of the initial value in order to prevent coolant boiling. After that, the flow rate was reduced again to 60% of the initial value and then kept constant.

In the RB2 test, power was increased from the initial linear power rating of 413 W/cm up to 1013 W/cm with the same ramp rate of 0.63 %Po/s as in the RB1 test. Even after the LOF onset, power was continuously increased to the 1047 W/cm until the reactor scram. In this test, the defect location was shifted upward from RB1 as mentioned above, in order to obtain higher temperature of fusible metal keeping the same margin to prevent the coolant boiling.

2-3. Summary of the test results

Based on the analysis of DN signal, slit opening was realized at 0.4 ± 1 second after LOF onset in the RB1 test. The radial cut at 40cm from BFC presented in Figure 3 shows that fractional fuel melting radius at the defect location is 0.45 Ro and that fusible metal has disappeared during transient. The radial cut at 46cm from BFC in Figure 4 shows fractional fuel melting radius of 0.57 Ro and the axial cut from 51.45 to 51.95 cm from BFC in Figure 5 shows 0.54 to 0.44 Ro melting.

Even with such considerable fuel melting, no meaningful molten fuel ejection or rapid gas release was observed from the expected time of slit opening until reactor scram. This means outer solid fuel shell prevented molten fuel ejection in case of the small fuel melting and slit opening type cladding failure. It is noted that clear DN signal increase was observed before the molten fuel ejection in spite of no meaningful gas release at the cladding failure time. It gives an encouraging aspect for anomaly detection with DN observation in the early phase of incidents.

In the RB2 test, it is likely that a leakage was formed at the cladding defect at 78.5 seconds after TOP onset. However, gas release after this leakage was very slow. Considering that PAPAS-2S calculation shows cladding mid-wall temperature at the defect location is ~400 ℃ which is rather lower than the melting temperature of fusible metal, this leakage is likely to have been consisting of a crack between the cladding and fusible metal. DN-signal increase after this time also indicates possibility of pin-failure detection before the molten fuel ejection. Flow, pressure and microphone signal changes were observed around 3.73 seconds after LOF onset. This event led to about 15 g of molten fuel ejection into the coolant channel above the defect location. On account of tight blockage around the defect location which was formed by the ejected fuel, flow rate finally decreased to the 8% of the initial value. It should be noted that coolant channel blockage observed in the RB2 test was a special case with the single pin geometry, and in the reactor case, there will be cooling from the neighboring coolant channels.

3. PAPAS-2S analysis for the RB1 and RB2 tests

In this chapter, PAPAPS-2S analysis for the fuel thermal conditions, especially for fuel melting in the RB1 and RB2 tests is described which is important for the interpretation of the RB1 and RB2 tests. However, the RB1 and RB2 tests with different power and cooling conditions provided a more extensive database for calibration together with the FAST ones.

3-1. Fuel-to-cladding gap conductance model

In the CABRI-FAST synthesis work, fuel-to-cladding gap conductance in the PAPAS-2S code was calibrated together with reduction of fuel thermal conductivity with local swelling through evaluation for the slow-TOP tests realized in the CABRI-FAST program. Within this work, the maximum gap conductance was set to 1.0 W/cm^2/K for the SCARABIX fuels throughout the transient. This maximum value was reached relatively early during the slow TOP transient.

In the present study for the CABRI-RAFT program, the slow TOP database increased with the RB1 and RB2 tests. In order to reflect this additional information, a new set of calibration is performed. In this new calibration, the maximum gap conductance is set to 0.5 W/cm^2/K before fuel melting and is set to 1.0 W/cm^2/K after reaching the fractional melting radius of 0.5. The maximum gap conductance between the melting initiation and the fractional melting radius of 0.5 is linearly defined from 0.5 to 1.0 W/cm^2/K. Although the maximum reduction of fuel thermal conductivity used for the slow-TOP tests in the CABRI-RAFT synthesis was 30% during the transient, it is set to 10% in the revised method. Using this revised method, recalculations for all the slow-TOP tests in the CABRI-FAST and RAFT programs are performed. Figure 6 shows comparison of fractional melting radius obtained from the experimental data and analytical result with the former and revised methods. The former method overestimates the fuel melting especially in RB1 and RB2 tests. On the other hand, the revised method shows better simulation for fuel melting in all the tests. Figure 7 shows comparison of average fuel enthalpy in between the former and revised methods. With the revised method, average enthalpy increases almost linearly in proportion to the linear power. On the other hand, with the former method, the average enthalpy becomes higher in the RB1 and RB2 due probably to the lower ramp rate and continuous heating after reaching the maximum power. Therefore the revised method is adopted in the following RB1 and RB2 calculations for the better simulation in fuel melting.

3-2. Analysis for the RB1 test

PAPAS-2S input data for the RB1 test is based on that of slow-TOP test in the

CABRI-FAST program which was commonly used in the PFX, PF1, and MF2 tests. Axial power profile, power and coolant flow rate history are well fitted to the experimental data as presented in Figures 8 to 10. In this study, two analytical cases with different gap conductance is introduced. RB1-MOD Case is the reference case based on the above-mentioned revised method. In addition to this case, RB1-1.4 Case with the maximum gap conductance of 1.4 $W/cm^2/K$ throughout the transient is also calculated.

Figures 11 and 12 show coolant temperature profile at steady state and coolant temperature history at TFC during the transient respectively. From these figures, it can be seen that all the analytical cases are in good agreement with the experimental data both in steady state and during transient.

Calculated fuel melting boundary after the transient based on the above-mentioned appropriate coolant thermal condition is presented in Figure 13 with experimental one which was obtained from the observation of radial and axial cuts. RB1-MOD Case shows reasonable simulation of the experimental data except at the defect location. On the other hand, considering that fuel melting at the defect location is consistent with the RB1-1.4 Case, fuel-to-cladding gap conductance is judged to have been locally higher at this location. This high gap conductance was due probably to lack of JOG which was evidenced by decrease of ^{137}Cs within the 3 cm around the defect location after the defect manufacturing in the ^{137}Cs axial profile before the transient as presented in Figure 14.

Reflecting the above mentioned effect, the total mass of molten fuel in the RB1 test is estimated to be ~ 24 g, based on the calculated result in RB1-MOD Case except for a 3 cm-height region at the defect location where that of the RB1-1.4 Case is adopted.

3-3. Analysis for the RB2 test

PAPAS-2S input data for the RB2 test is based on that of RB1 test. Power history is well fitted to the experimental data as presented in Figure 15. The same coolant flow reduction history as in the RB1 test is adopted in the analysis.

Figures 16 and 17 show the coolant temperature profiles during steady state and the coolant temperature history at TFC during the transient, respectively. These figures show that calculated coolant temperature is consistent with the experimental data both at steady state and during the transient.

Calculated fuel melting boundary at the final state is shown in Figure 18 compared with the experimental data which was obtained from the thickness of solid fuel shell in the radial and axial cuts, and shows reasonable agreement with this experimental data. Based on this result, calculated fuel melting boundary just before the molten fuel ejection is obtained and presented in Figure 18. The total mass of molten fuel is estimated to be ~ 55 g based on the calculated fuel melting boundary.

Concerning the Pellet Cladding Mechanical Interaction (PCMI), no cladding plastic strain was calculated before the molten fuel ejection. This shows that SCARABIX-CABRI type fuel pin has large margin to the pin failure under the realistic conditions without defect; this was also confirmed in the slow-TOP tests in the CABRI-FAST program.

4. Interpretation of the test results based on the experimental data analysis

In this chapter, interpretation of the both tests is given based on the detailed experimental data analysis and fuel melting evaluation described in the chapter 3.

4－1. Interpretation of the RB1 test

In the RB1 test, slit opening was realized at 0.4 ± 1 second after LOF onset. This timing was obtained from the DN signal with the consideration of transit time which is presented in Figure 19. It should be noted that this transit time is obtained on assumptions that the neutron emitter speed is equal to the average sodium velocity and that coolant mixing effect is negligible. Besides, the uncertainty of the ± 1 second is on account of the volumes of the different sections of the CABRI sodium loop and the varying sodium flow rate.

The DN signal increases to a considerable level at the beginning of the pin failure, and furthermore it rises up to approximately 3 times of this level.

The radial cut at 40 cm from BFC after the transient shows no fusible metal as presented in Figure 3. In addition, deduced from the deformation of the Ni coating this fusible metal has melted away during the transient. Observed several radial cracks are considered to have been closed during the transient because of no evidence of molten fuel invasion into these cracks. On the other hand, taking account of no meaningful change on signals in flow meter, pressure transducer, void detector, and microphone, it is concluded that there was no meaningful molten fuel ejection or gas release before the SCRAM. It is noted that there might be very slow gas release on account of small oscillation of inlet and outlet flow rate from 61.4 seconds after LOF onset until SCRAM in Figure 20. This is considered to be due to the mitigation of cladding constraint against the fuel after the cladding temperature increase caused by further flow reduction from 30 to 60 seconds after the LOF onset. Thus, RB1 test shows that molten fuel ejection and rapid gas release can be prevented under the conditions of limited fuel melting and slit-type cladding failure.

Figure 21 shows axial ^{106}Ru profile before and after the transient. Based on the knowledge obtained in the past CABRI tests, it is well known that ^{106}Ru separates and educes after the fuel melting, and it accumulate at the penetrated edge when molten fuel moves axially within the central hole. Therefore it is deduced that molten fuel moved from 0 to 68 cm from BFC. Considering axial melting extension from 22 to 59 cm from BFC calculated in the PAPAS-2S analysis, it is understood that molten fuel moved both upward and downward through the central hole.

On the other hand, after the SCRAM which corresponded approximately to 70 s after LOF onset, flow rate change due probably to relatively rapid gas release was observed as presented in Figure 22. It is presumed that fuel shrinking and relaxation of cladding constraint due to the fuel temperature decrease after the SCRAM caused this gas release.

Flow rate changes indicate two peaks of gas release at 2.9 and 3.6 seconds after the SCRAM. The maximum difference between inlet and outlet flow rate is 0.23m^3/h. Compared with the maximum difference between inlet and outlet flow rate of 1.0 and 1.5 m^3/h in the E11 and E13 tests in the CABRI-II program, this is rather small. On assumption that this flow rate change is due to the gas release, that gas mainly consist of plenum gas such as Xe and Kr, and that this gas temperature is equivalent to the coolant temperature, the maximum gas release velocity is estimated to be 0.4g/s at 3.6 seconds after the SCRAM. However, it should be noted that the resistance against the upper plenum gas blowout was lower in these CABRI-II tests because the failure locations were near the TFC and there was no upper blanket. On the other hand, with the defect located in the axial center in the RB1 test, large resistance against the upper and lower plenum prevented rapid gas blowout. Therefore, it should be noted that more rapid plenum gas blowout after the SCRAM might occur depending on the failure location.

4 — 2. Interpretation of the RB2 test

In the RB2 test, leak failure at the defect location has occurred at ~ 78.5 seconds after the TOP onset (~ 619 W/cm at PPN), when inlet and outlet flow rate have changed as presented in Figure 23, and when the DN signal correlated by the transit time has increased as shown in Figure 24.

Time integration of the flow rate difference between coolant outlet and inlet leads approximately to ~115 cm^3 of the differential volume. If we assume that the released gas is responsible for this and that the gas temperature and pressure in the coolant channel are 350 ℃ and 3.5 bar respectively, the released gas is estimated to be ~180 cm^{3}STP. It should be noted that the flow rate deviation decreases after the probable leakage formation. On the other hand, fuel melting is expected at about 140 sec into the transient. This suggests that the gas release path from the plenum to the failure site, which will have consisted of narrow crack system within the still solid fuel and/or fuel-to-cladding gap, decreased during the power increase phase. It is also probable that molten fuel invasion into the narrow path formed a blockage and prevented farther gas release. On the other hand, total plenum gas volume at the time of gas release is estimated to be ~230 cm^3 based on the plenum gas volume of 348 cm^{3}STP in the SCARABIX-CABRI type pin. Therefore, large amount of plenum gas will have still remained in the upper and lower gas plenum before the molten fuel ejection. This is consistent with the fact that a large amount of gas was released at the time of molten fuel ejection and subsequent upper and lower plenum gas blowout which will be described hereafter. Therefore, it can be concluded that the rather early gas leak occurred in this test did not give significant impact on the subsequent behavior.

On the other hand, it is encouraging from the viewpoint of failure detection that the meaningful DN signal increase was observed even in such a slow gas release.

Large flow divergence was observed at ~ 3.74 seconds after LOF onset as presented in Figure 25. Then, about 20 ms after this time, microphone and pressure transducer signals showed large peaks as shown in Figures 26 and 27. Furthermore, approximately 70 ms after this time (~ 3.84 seconds after LOF onset), microphone and pressure transducer signals showed similar large peaks. Detailed analysis for these events are performed and presented in the following paragraphs.

Figure 28 shows voiding zone extension in the coolant channel which was obtained from the time integration of flow rate with the information of thermocouples installed in the coolant channel. This voiding zone extension shows consistency with the coolant temperature increase. Molten fuel ejection was detected from the observation of hodoscope signal increase at about 3.74 seconds after LOF onset. Then, approximately 20 ms after this time, FCI and coolant channel voiding occurred. At about 70 ms after this voiding initiation, flow recovery and rewetting at the defect location took place as seen in this figure. A continuous molten fuel ejection which can be observed at this time in the hodoscope signal (shown in Figure 29) and it led to a second FCI accompanied with second microphone and pressure transducer signal peaks.

On basis of the Hodoscope data analysis, fuel ejection in the coolant channel took place between 48.9 and 53cmBFC. Fuel mass in the coolant channel can be deduced assuming some fuel geometry. If we assume that the fuel within the pin is same as the initial value, ejected fuel within the coolant channel in this axial zone is estimated to be 7.2g. However, calculated molten fuel amount in this axial zone is 4.5g (PAPAS-2S result). Therefore, if we assume that the molten fuel within the cavity is absent, ejected fuel within the coolant channel in this axial zone is estimated to be 11.7g. It should be noted that these values of estimated fuel mass does not include the uncertainty of the measurement itself.

There is also a small signal increase suggesting a potential presence of fuel in the coolant channel above this level between 59.2 and 71.5cmBFC. The summation over this height of the amount of fuel present in the coolant channel gives an estimated fuel amount of ~5 g at ~200 ms.

Therefore, it is considered that an initial fuel ejection leading to ~15g of ejected fuel mass took place within ~200ms.

Fuel ejection velocity is estimated to be ~0.075 g/ms from the hodoscope signal analysis which is relatively slow compared with the 0.1 to 0.2 g/ms in the CABRI-FAST E12 and BCF1 tests. This is considered to be due to the lower molten cavity pressure in the RB2 test where low smear density fuel was used than in the E12 and BCF1 tests where high smear density fuel was used.

Coolant voiding extension due to gas release and FCI in the RB2 test is shown in Figure 30 together with other CABRI tests. The voiding extension speed in the RB2 test is also slower than that in the E12 and BCF1 tests. Therefore, not only the fuel ejection velocity but also the FCI and gas release behavior can be mitigated with the low smear density fuel.

Coolant saturation temperature at 30 and 45 cm from BFC increases up to

1040 ℃ as presented in Figure 31 due to about 3 bar inlet pressure increase (shown in Figure 27) through the two FCI events. This saturation temperature increase indicates considerably tight blockage formation. This is consistent with the signal increase within about 10 cm just above the defect location in the axial profiles of ^{154}Eu gamma scanning, hodoscope signal after the transient, and X-ray radiography presented in Figure 32. It is also consistent with small permeability of the accumulated fuel in the coolant channel observed in the axial cut from 49 to 52.5 cm from BFC shown in Figure 33.

After the molten fuel ejection, oscillation of outlet void detector signal was observed as shown in Figure 34 and it can be interpreted as passing of non-condensable gas because the coolant temperature at the void detector was below the coolant saturation temperature. This continuous passing of non-condensable gas for a few seconds indicates slow gas release from the gas plenum.

Figure 35 shows fuel ejection and coolant channel void development behavior derived from the above presented information. With the single pin geometry in CABRI, coolant channel can be easily blocked. However, it should be noted that even under such condition the coolant channel temperature does not exceed the saturation level for a few seconds after the fuel ejection except for the very short time period at the beginning. This suggests that the coolant channel keeps its wet characteristic which is important for prevention of rapid failure propagation. In the reactor case, the liquid coolant present in the neighboring sub-channels will provide significant cooling so that long term coolability may be obtained. However, in the RB2 test condition, absence of such cooling inevitably resulted in liquid sodium starvation and dryout. With this dryout, cladding temperature started to increase rapidly leading to significant reduction of its constraint against fuel stack.

Hodoscope signals in the upper part of the fissile region decreased from about 6.2 seconds after LOF onset with the rapid signal increase of the displacement transducer as presented in Figure 36. In addition to this, there was also a large inlet and outlet flow divergence at this time. Furthermore, void detector signal shows continuous voiding after this event. Based on these pieces of information, it is considered that a relatively rapid gas release from the upper plenum has occurred. It is expected that the cladding temperature became higher before this event judging from the fact that coolant temperature from 45 to 60 cm from BFC exceeded saturation temperature as presented in Figure 35. In addition, the large oscillation of displacement transducer suggest that the cladding was divided into upper and lower parts at the failure location, and as a result, plenum gas pressure pushed pin top upwards and pushed fissile top downwards. ^{60}Co gamma scanning presented in Figure 37 shows steel decrease around the defect location and accumulation below the lower fissile part. Radial cut at 38.6 cm from BFC presented in Figure 38 shows also large steel accumulation. Therefore, cladding around the defect location has melted and moved downward after this event.

After the SCRAM of 6.8 seconds after the LOF onset, lower plenum gas was released at about 7.5 seconds after LOF onset accompanied with the signal change of inlet flow meter (Figure 25) and inlet void detector as presented in Figure 34. Accompanied with this gas release, lower fissile part was pushed upwards by the lower plenum gas pressure leading to a slide up by 12.8 cm which was evidenced from the hodoscope signal (Figure 29) and ^{154}Eu gamma scanning after the transient (Figure 32).

5. Discussion

Very useful information related to behavior of the molten fuel ejection, preventing mechanism against such ejection, coolability of the ejected molten fuel, plenum gas release behavior, and failure detection by DN detector were obtained from the interpretation of the RB1 and RB2 tests. The possible impact of fuel smear density on fuel ejection behavior, threshold for fuel ejection and plenum gas release behavior is discussed below as well as consideration for the coolability of the ejected molten fuel and failure detection by DN detector.

(1) Threshold of the molten fuel ejection

It is confirmed through the CABRI-FAST program that the low smear density fuel has larger margin to the pin failure compared with the high smear density fuel. In addition to this, RB1 test showed prevention against the molten fuel ejection with the low smear density fuel even under the condition of the cladding failure accompanied with the maximum fractional melting radius of 0.57 Ro. On the other hand, cladding failure and molten fuel ejection occurred without a defect under similar melting condition in the CABRI-II E12 and BCF1 tests with high smear density fuels. Therefore, the low smear density fuel has larger margin to the molten fuel ejection compared with the high smear density fuel. On the other hand, a more extensive fuel melting condition was reached (0.67±0.05 Ro) in the RB2 test leading to a very thin solid fuel shell outside the molten fuel cavity and realized molten fuel ejection.

(2) Behavior of molten fuel ejection and gas release

In the E12 and BCF1 test, velocity of the molten fuel ejection is more than twice than that in the RB2 test. RB2 test showed molten fuel ejection became relatively slow with the low smear density fuel reflecting the low molten cavity pressure. This result suggests that low smear density fuel may lead to reduced potential of failure propagation.

(3) Coolability of ejected molten fuel

Although coolant temperature exceeds saturation temperature momentarily after the molten fuel ejection in the RB2 test, all thermocouples show coolant temperature stays below the saturation level for 1 to 2 seconds as shown in Figure 39. Since the RB2 test is performed in the single pin geometry, flow has not recovered within the short time period with the coolant channel blockage. However, the coolability from the neighboring coolant channel becomes important in the reactor case. Although RB3 test was expected in the earlier schedule which was aiming to clarify the effect of coolability from neighboring coolant channels, it was canceled due to the non-availability of the SCARABEE reactor. From the viewpoint of coolability in the bundle geometry, the J1 and R12 tests which were performed with 7-pin bundle geometry in the US TREAT reactor give useful information. Slow-TOP transient leading to pin failure was realized in the J1 and R12 tests with the fuel burn up of 7 and 0 at.%, respectively. Despite ejected molten fuel of approximately 50 and 60 g in the J1 and R12 tests, respectively, more than 90 % flow recovery was confirmed as shown in Figure 40. Based on these pieces of information, it can be said that there is a certain possibility to establish a coolable condition in the bundle geometry of the reactor case provided that the ejected fuel mass including that from the neighboring pin if any does not exceed the RB2 test situation.

(4) Behavior of plenum gas release

No plenum gas release was likely before the reactor scram with the closed fuel-to-cladding gap condition after the molten fuel ejection in the E12 and BCF1 tests where high smear density fuels were used. On the other hand, plenum gas release within a few seconds after the molten fuel ejection was likely in the RB2 test with the low smear density fuel. Therefore, plenum gas could be released more rapidly with the low smear density fuel compared with the high smear density fuel due to the PCMI mitigation effect.

(5) Failure detection

In the RB1 test, DN precursor emission into the coolant channel just after the cladding failure was confirmed by the DN detectors installed in the coolant channel. In the RB2 test, DN signal increase was observed just after the leakage formation before the fuel melting. These pieces of information suggest the high potential of anomaly detection by DN detector before fuel melting and ejection.

6. Conclusions

Interpretation for the RB1 and RB2 tests based on the detailed evaluation of the experimental data and PAPAS-2S code analysis were performed in this study. Furthermore, through the comparison with CABRI-II experiment, the possible impact of the fuel smear density on fuel ejection behavior, threshold for fuel ejection, and plenum gas release behavior was evaluated.

This study indicated that molten fuel ejection can be prevented with the low smear density fuel under a small amount of fuel melting and slit-type cladding defect. On the other hand, fuel ejection is likely in a case of very thin solid fuel shell surrounding the molten fuel cavity. However, the rapidness of the fuel ejection with the low smear density fuel is less pronounced compared with that of the high smear density fuel. It should be noted that the coolant channel basically was still filled by liquid sodium in the RB2 test in the early phase of post-fuel ejection. This fact is encouraging with respect to coolability of the ejected fuel. Moreover, considerable DN-precursor release into the coolant flow already before fuel ejection is regarded as useful for consideration of anomaly detection with DN signal observation.

Table 1 SCARABIX-CABRI type fuel characteristics

Fuel fissile length	750mm
Upper blanket length	30mm
Lower blanket length	20mm
Upper plenum length	286mm
Lower plenum length	213mm
Cladding outer diameter	8.5mm
Cladding inner diameter	7.37mm
Fuel outer diameter	7.134mm
Fuel inner diameter	2.03mm
Cladding material	15-15Ti
Fuel linear mass	3.853g/cm
O/M ratio	1.982

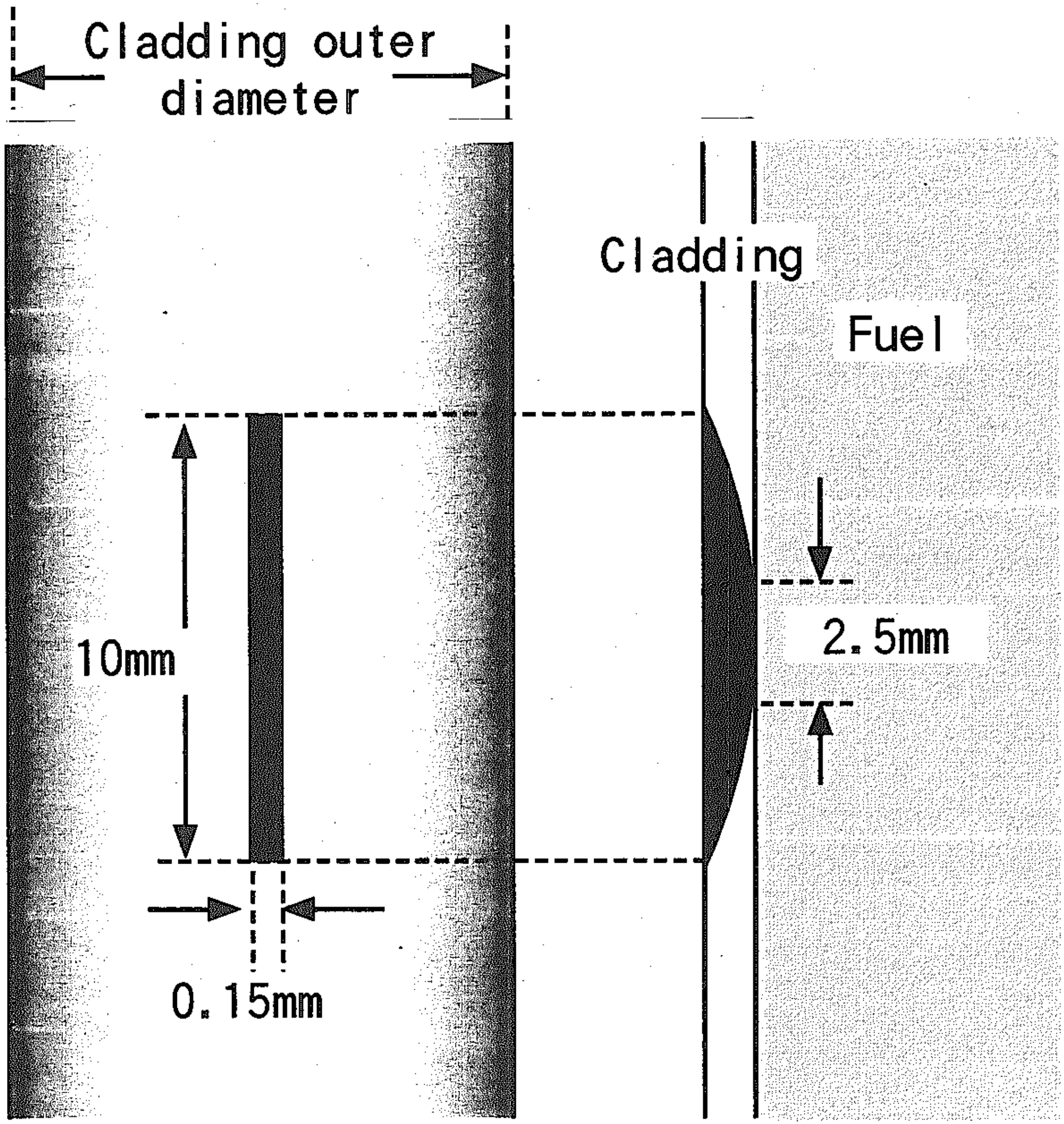

Figure 1 Simplified drawing of the notch in the RB1 and RB2 tests

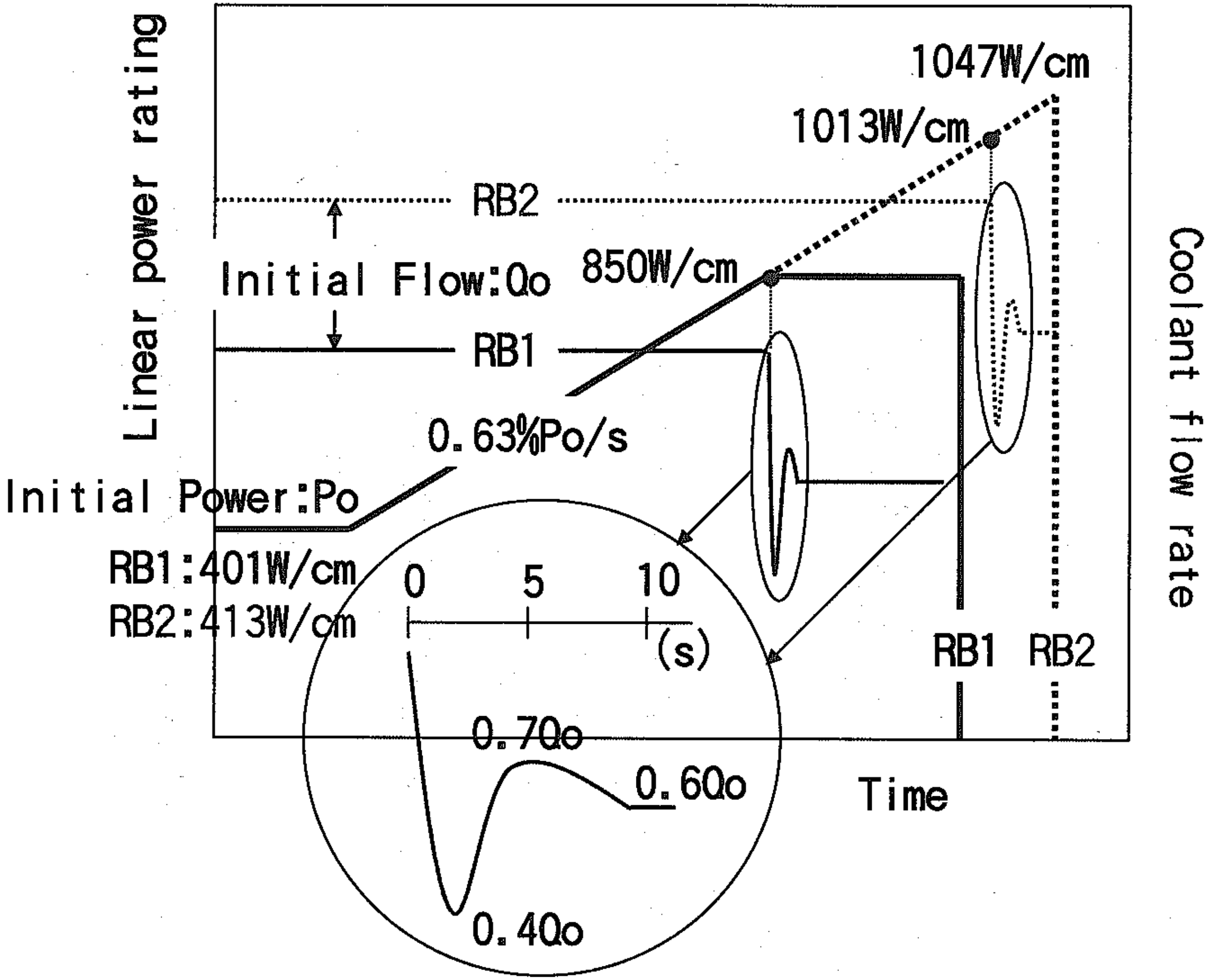

Figure 2 Power and flow history in the RB1 and RB2 tests

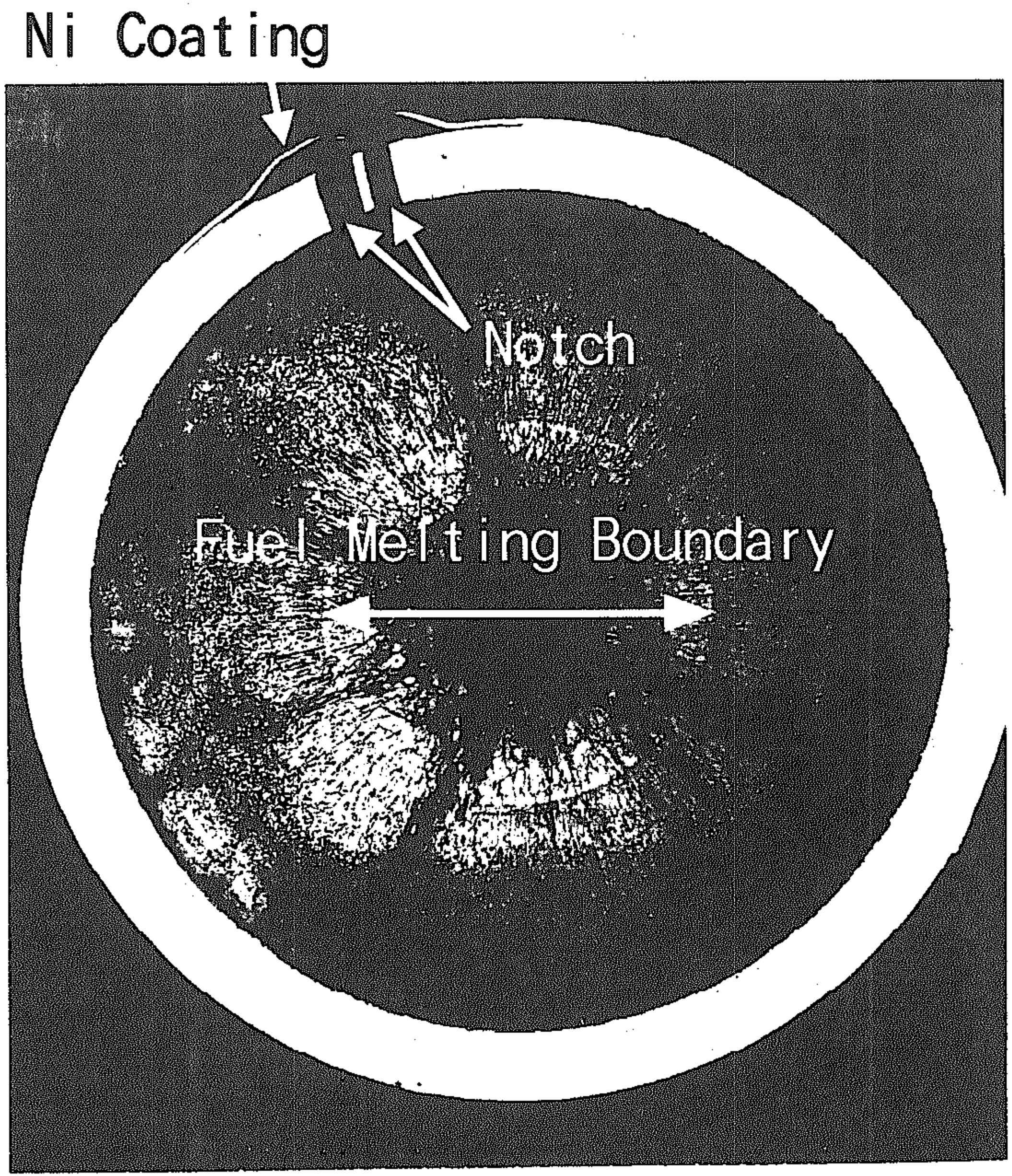

Figure 3 Radial cut of the RB1 test pin at 40cm from BFC

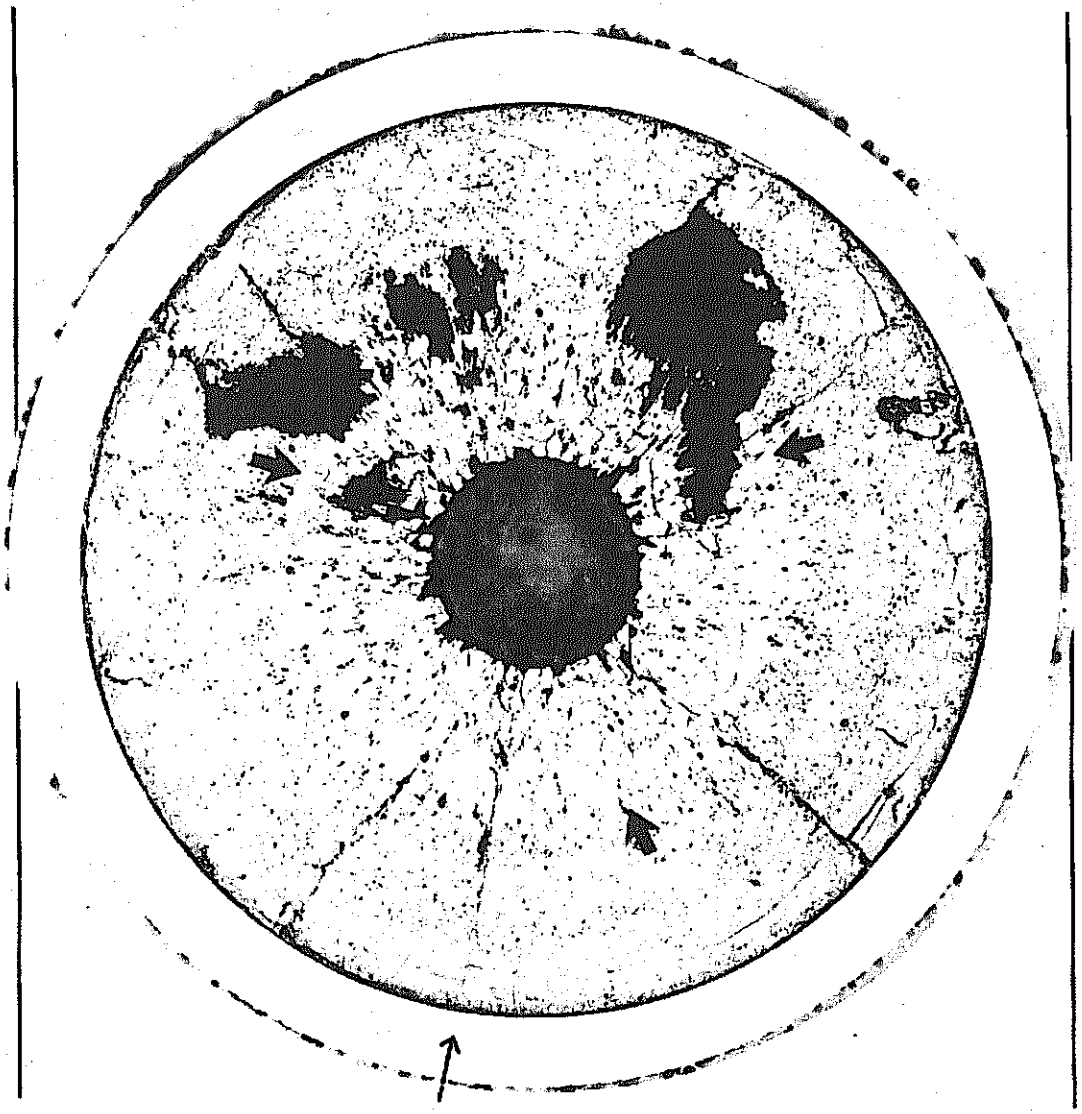

Figure 4 Radial cut of the RB1 test pin at 46cm from BFC

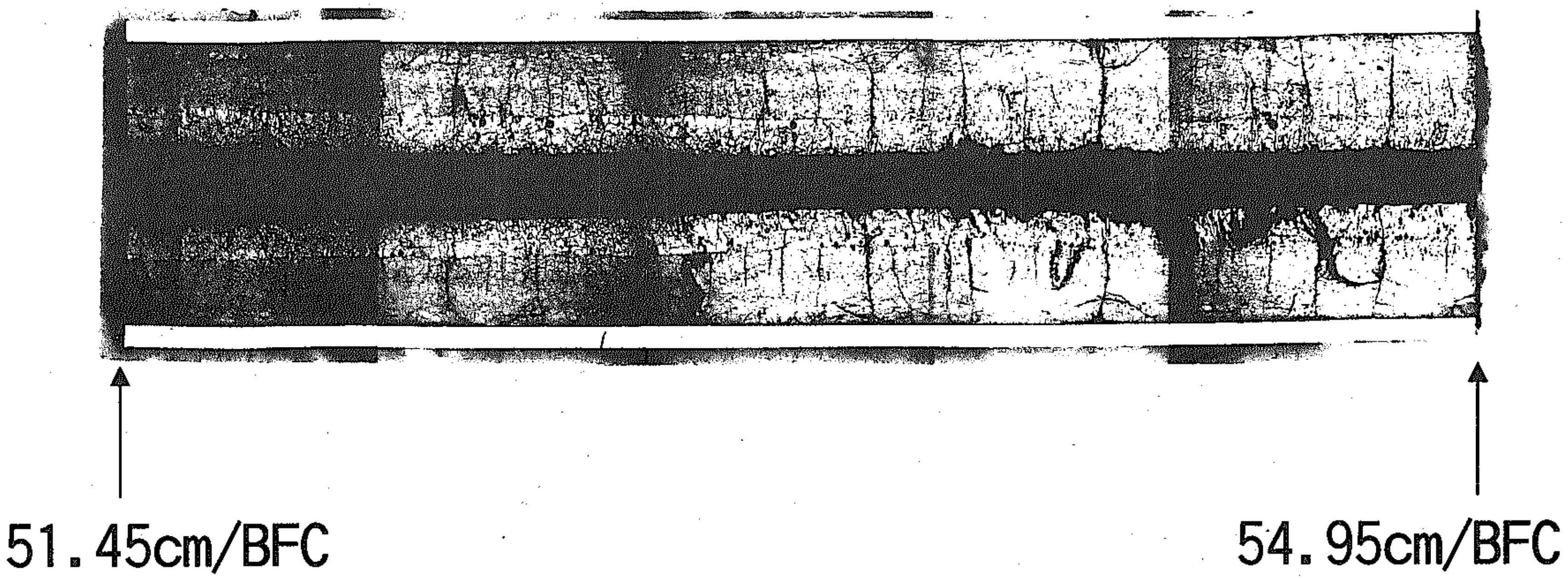

Figure 5 Axial cut of the RB1 test pin
from 51.45 to 54.95 cm from BFC

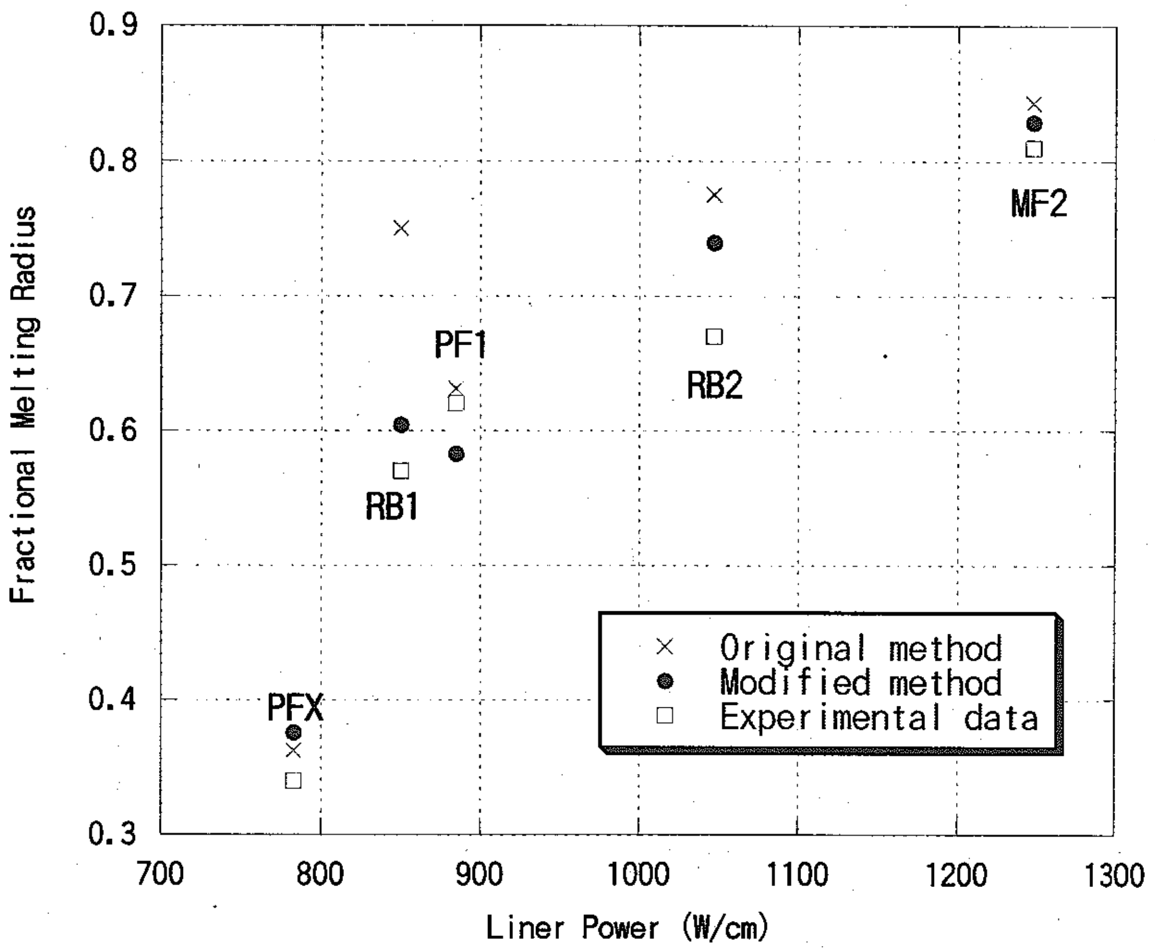

Figure 6 Fractional melting radius in the FAST and RAFT slow-TOP tests

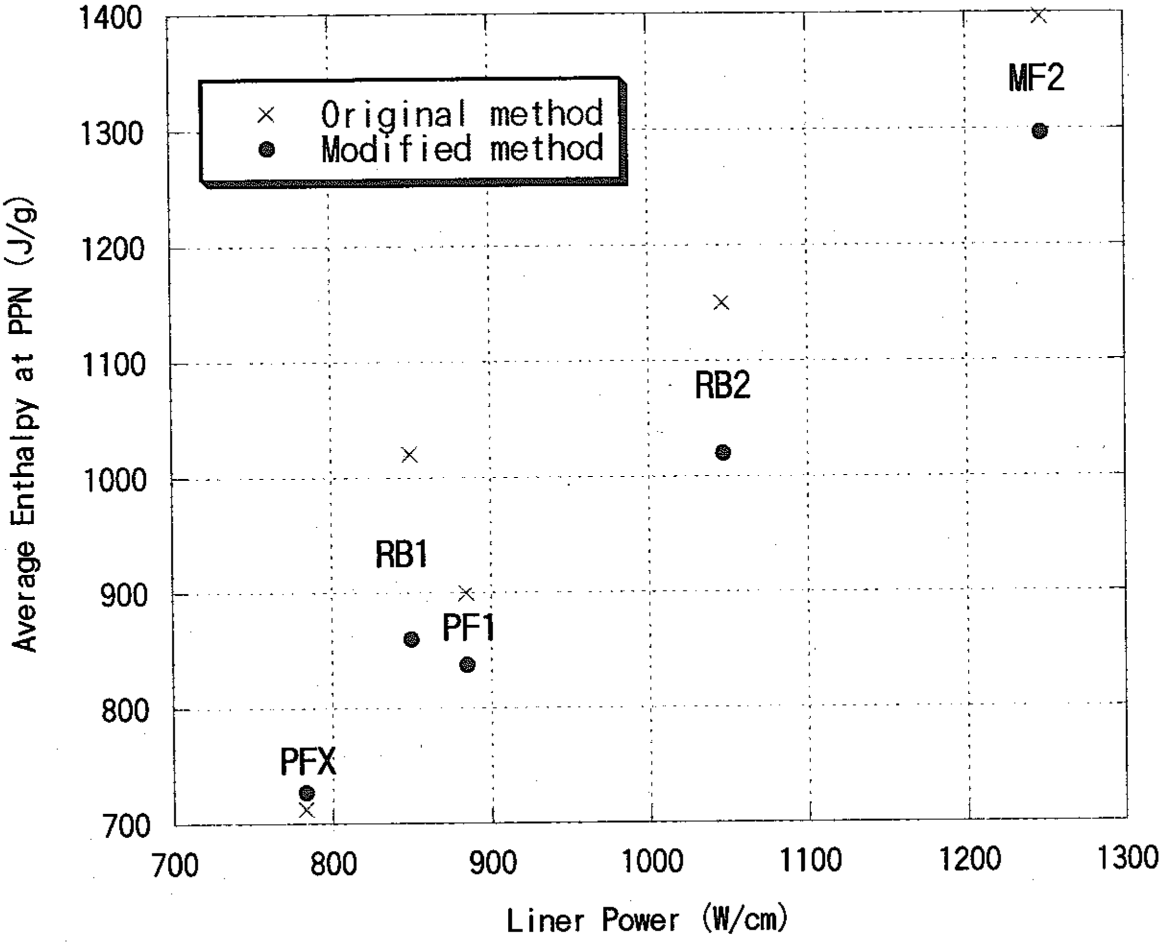

Figure 7 Average enthalpy at PPN in the FAST and RAFT slow-TOP tests

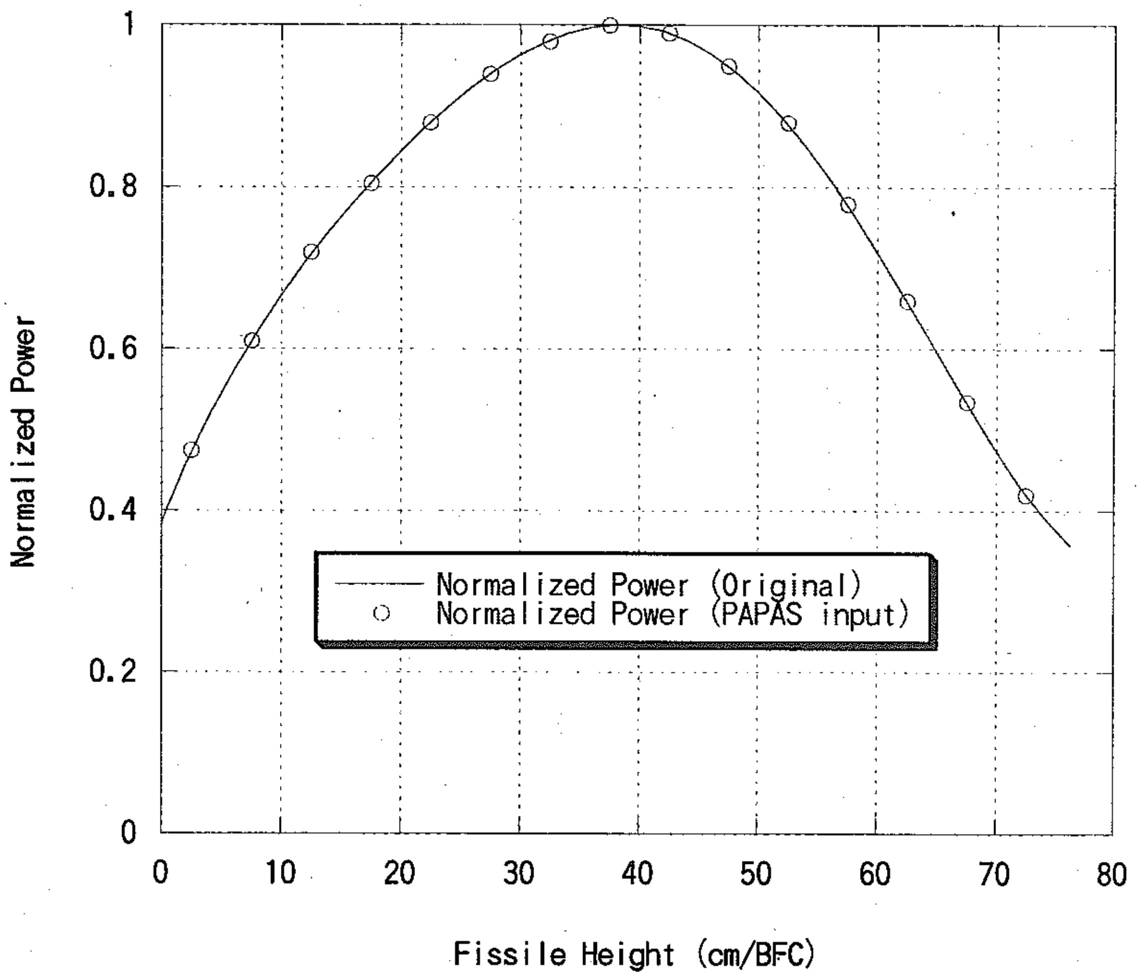

Figure 8 Axial power profile of the RB1 test fuel

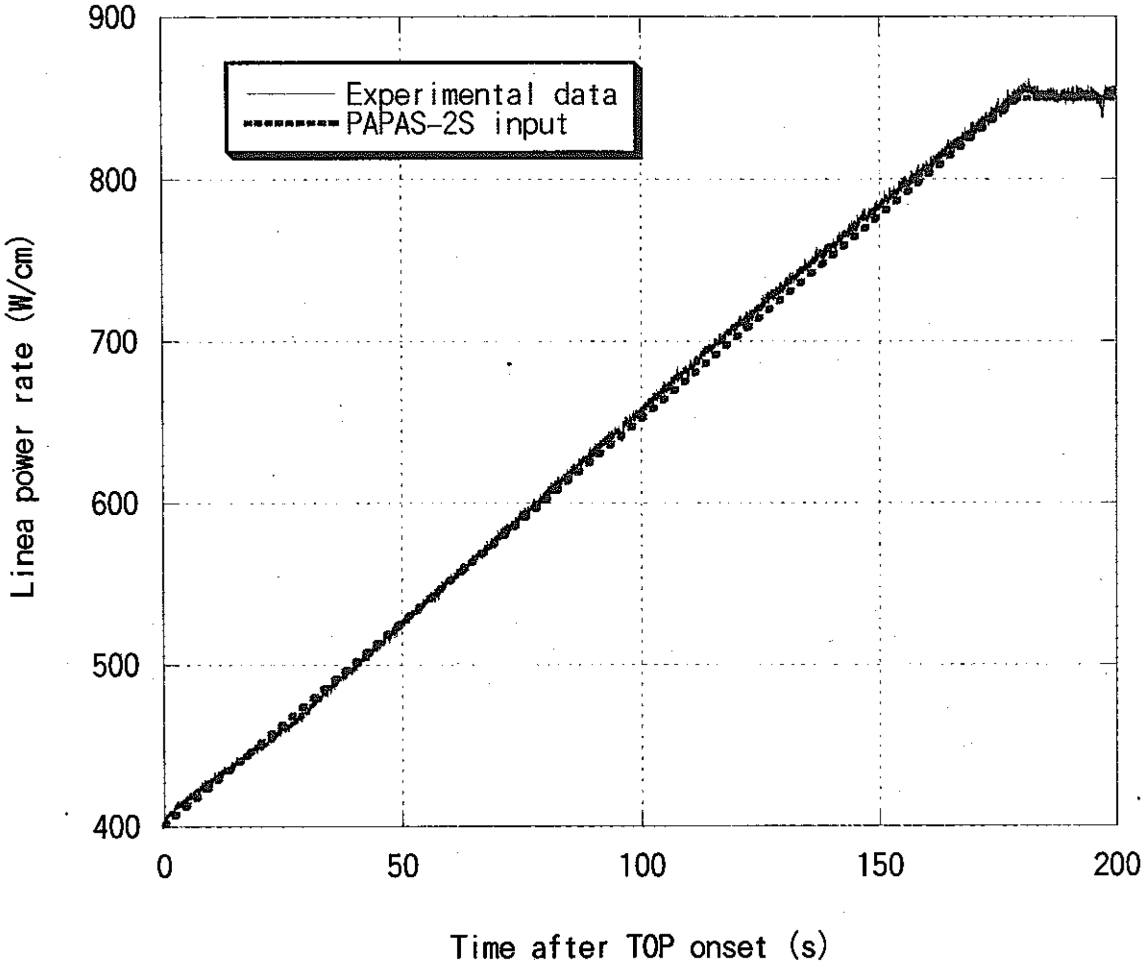

Figure 9 Power history of the RB1 test used in the PAPAS-2S analysis

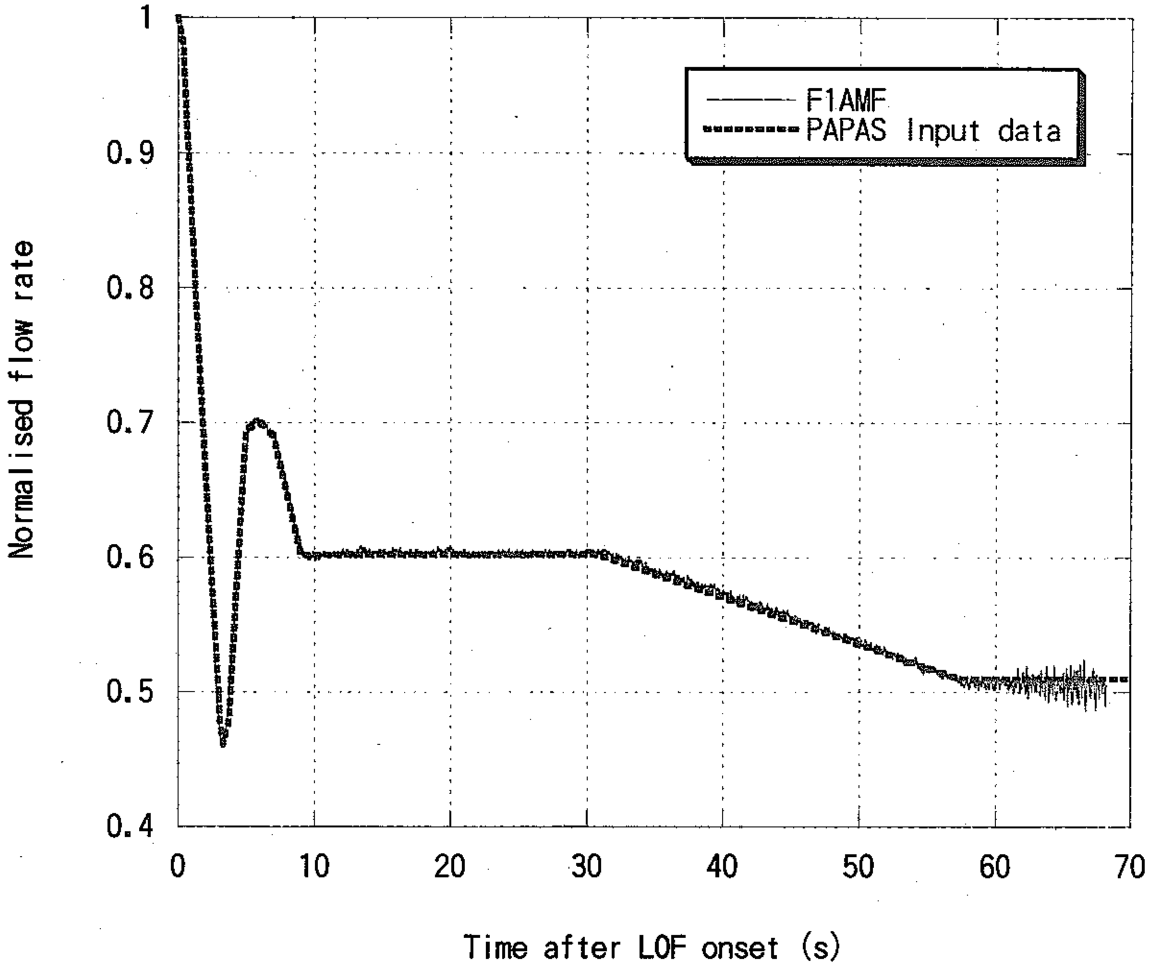

Figure 10 Coolant flow history of the RB1 test used in the PAPAS-2S analysis

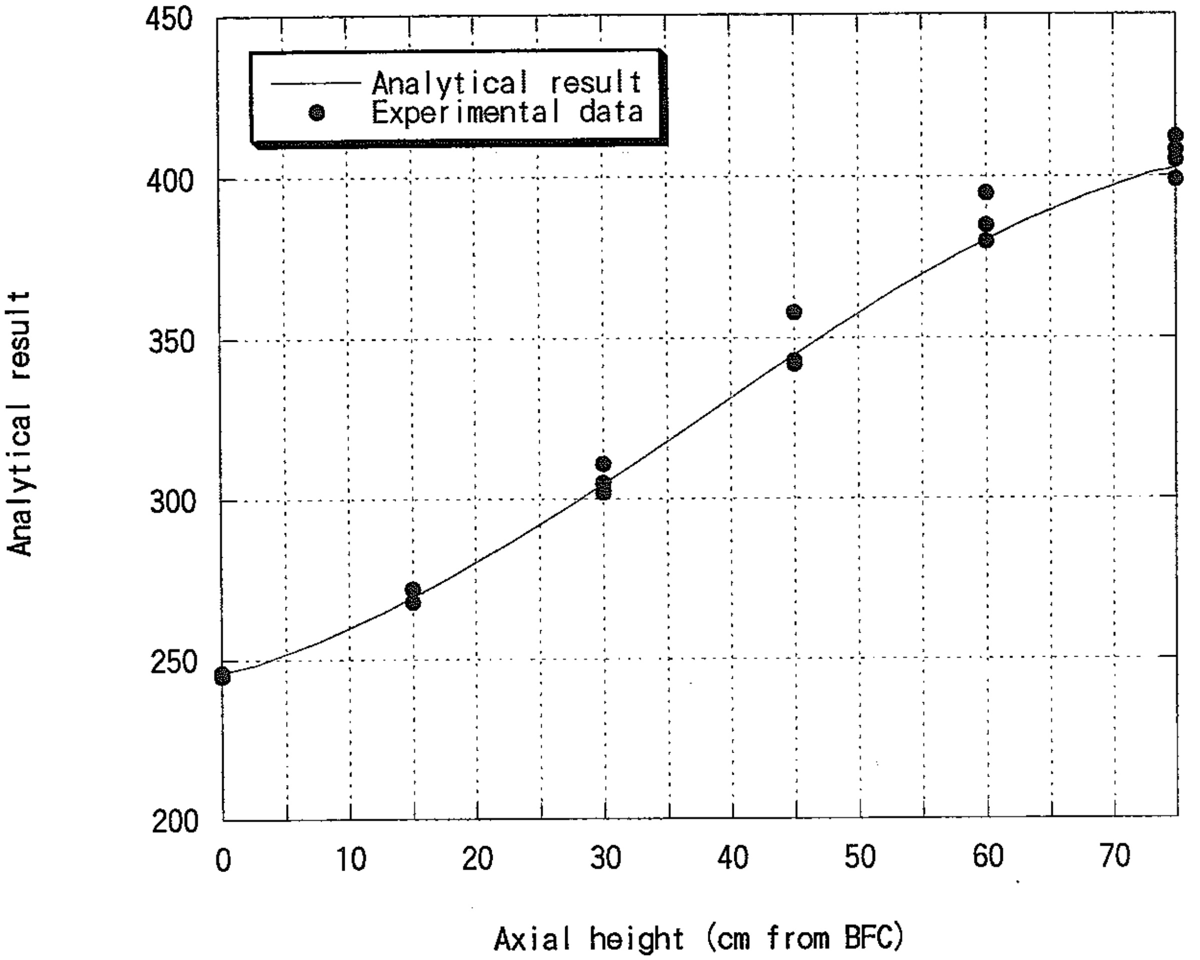

Figure 11 Comparison of coolant temperature profile at steady state in the RB1 test

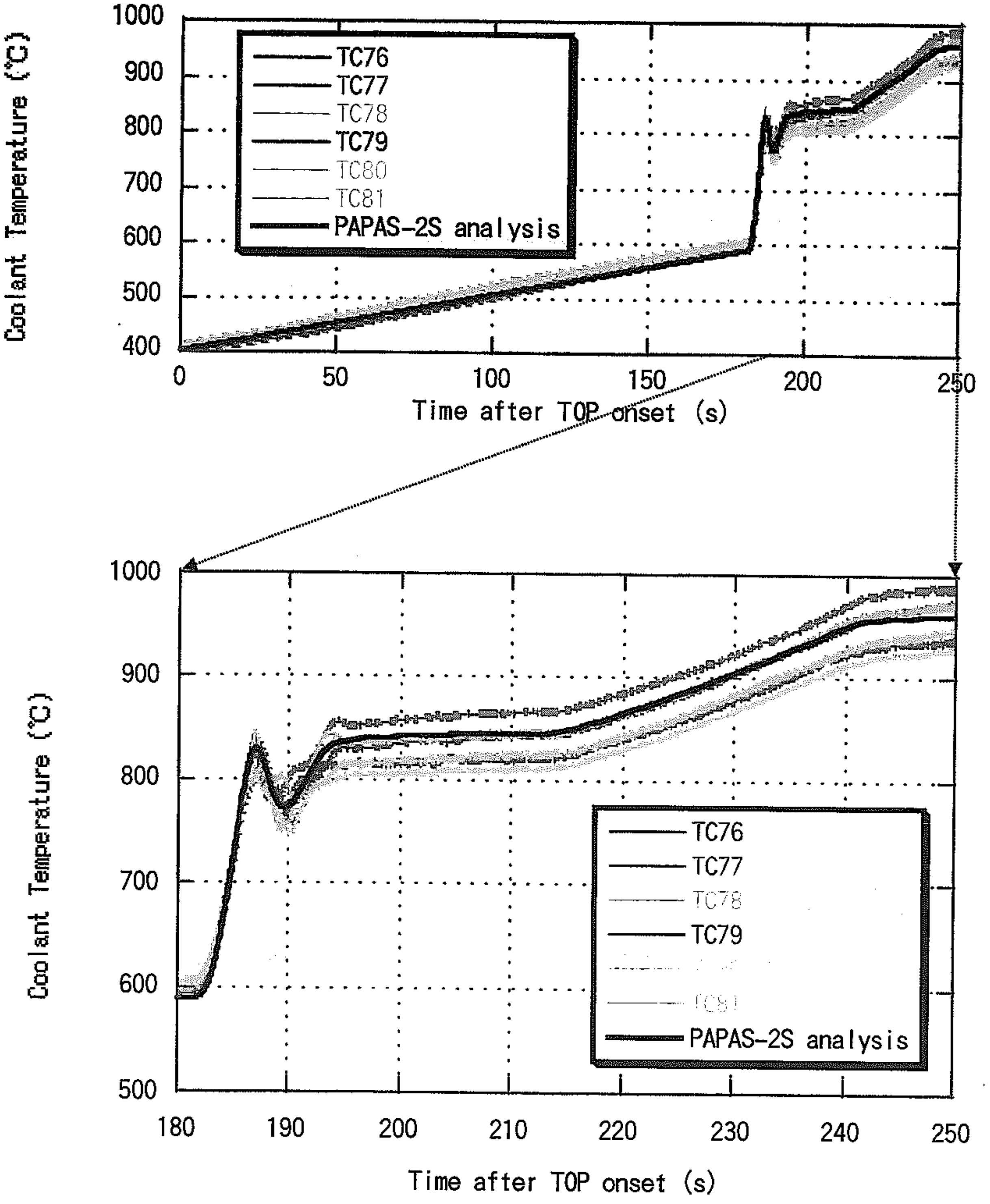

Figure 12 Comparison of coolant temperature history at TFC in the RB1 test

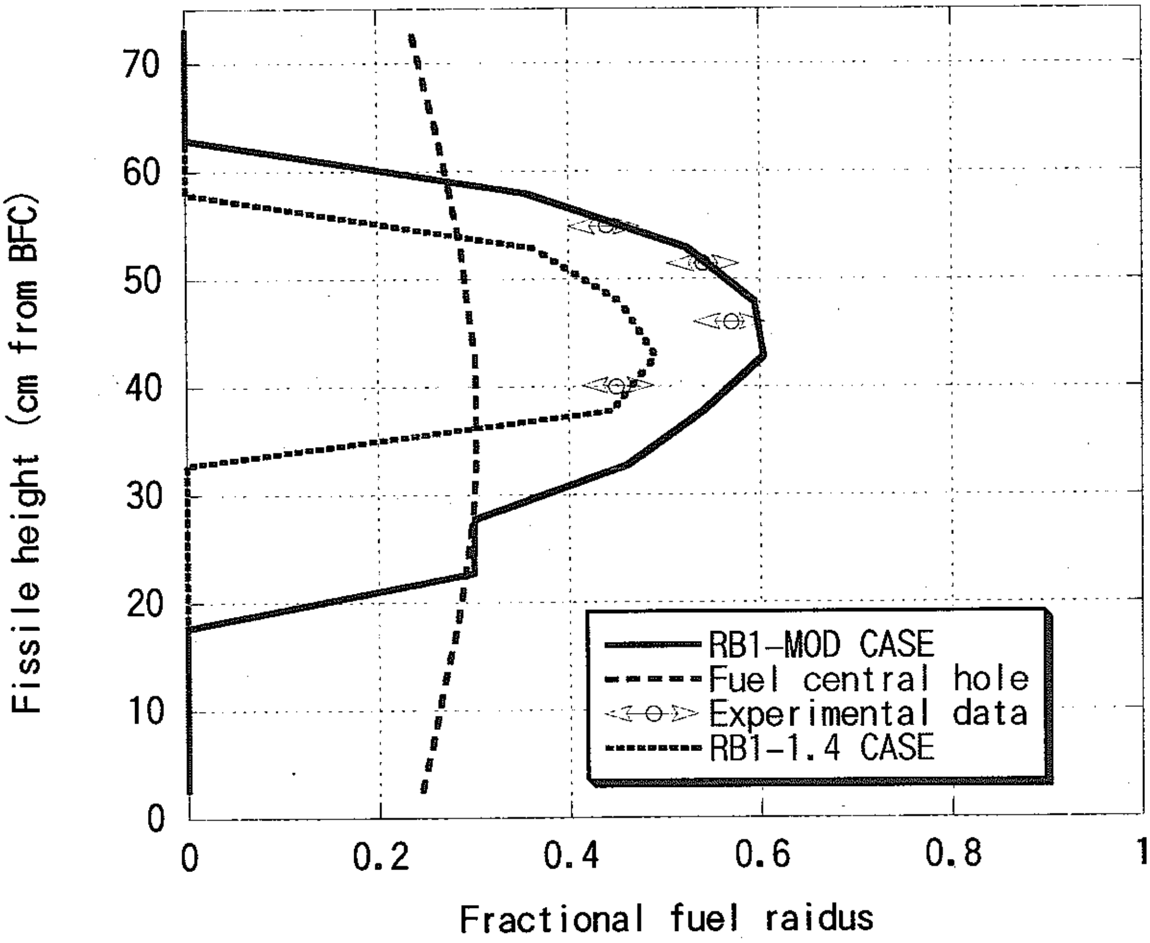

Figure 13 Comparison of fuel melting boundary in the RB1 test

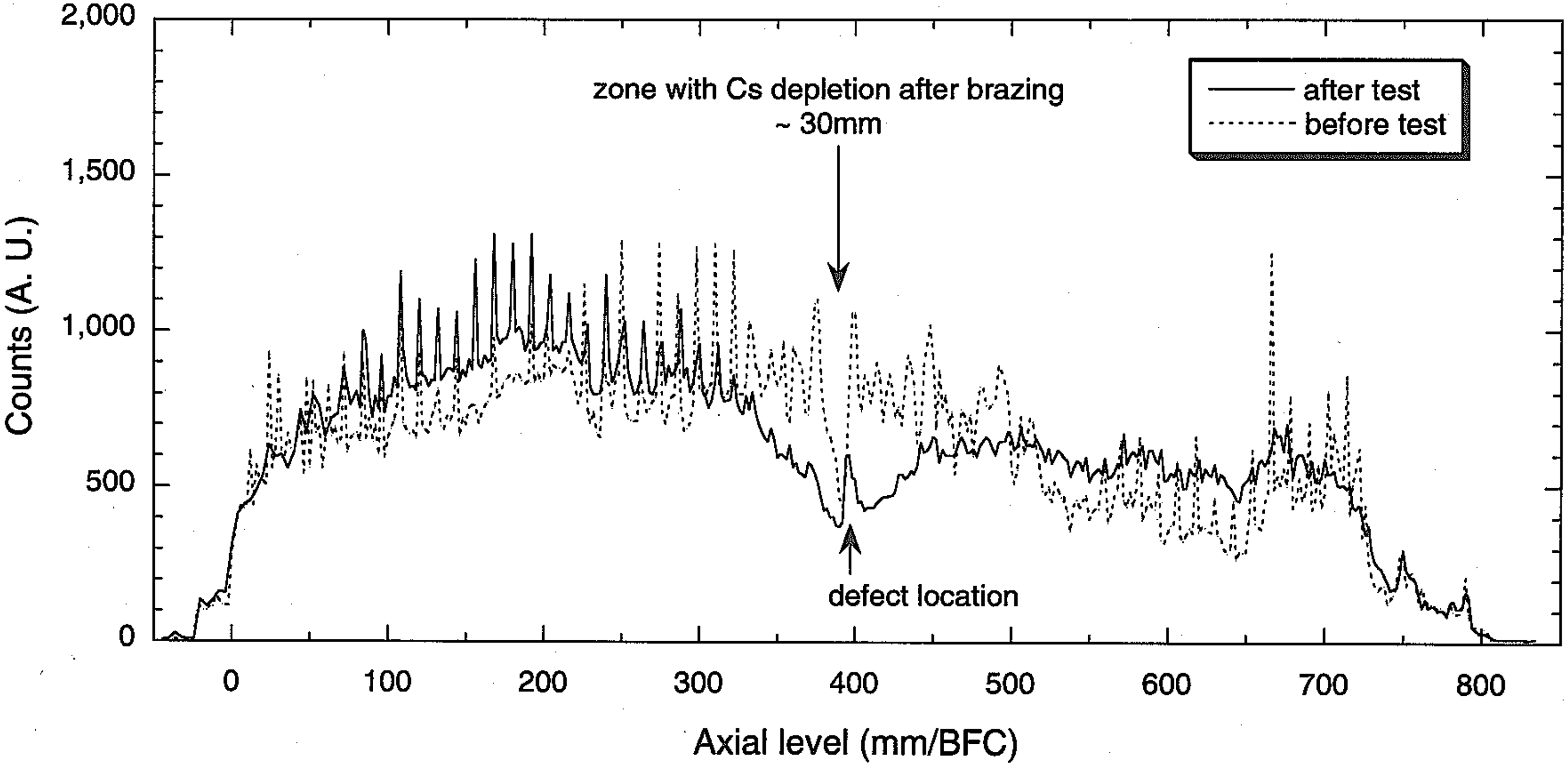

Figure 14 ^{137}Cs axial profile before and after the RB1 test

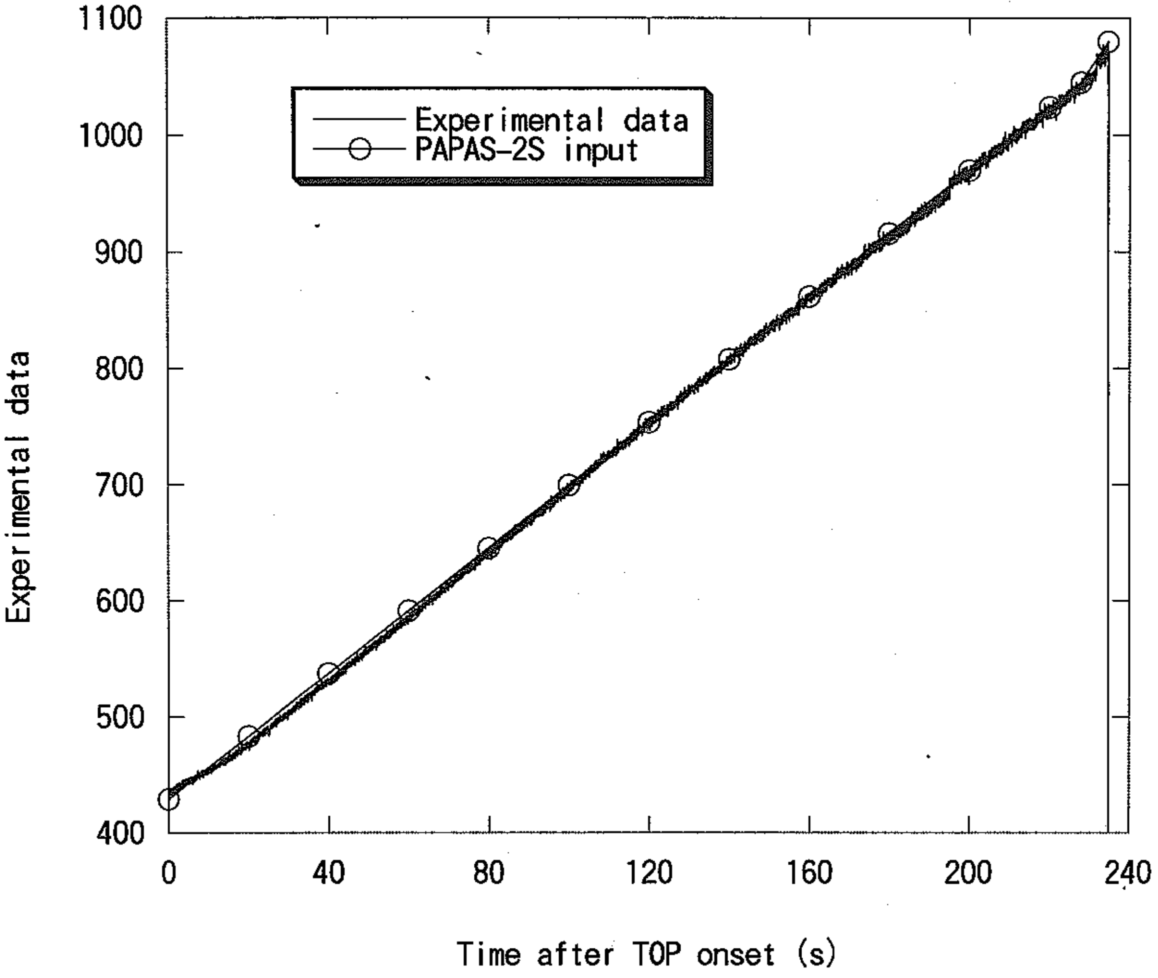

Figure 15 Power history of the RB2 test used in the PAPAS-2S analysis

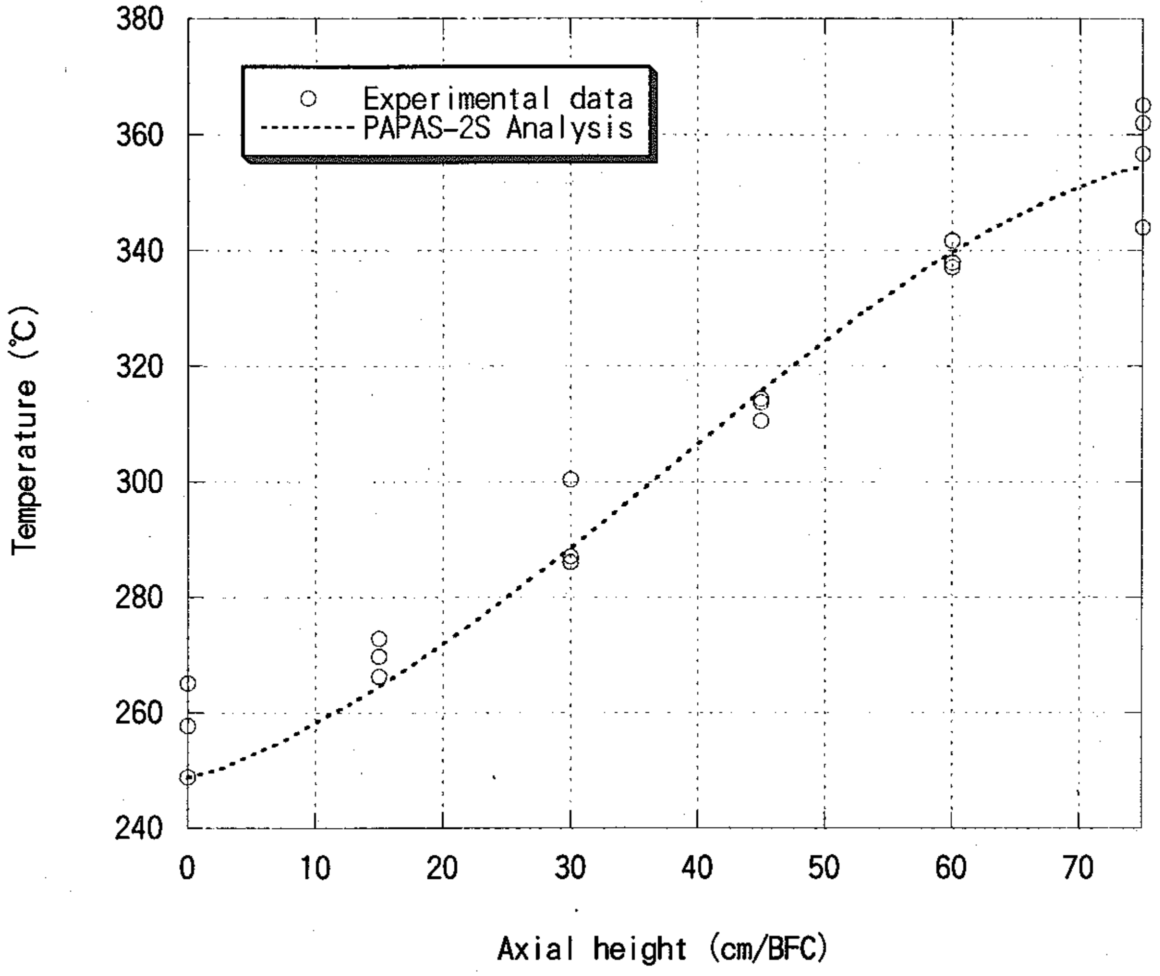

Figure 16 Comparison of coolant temperature profile at steady state in the RB2 test

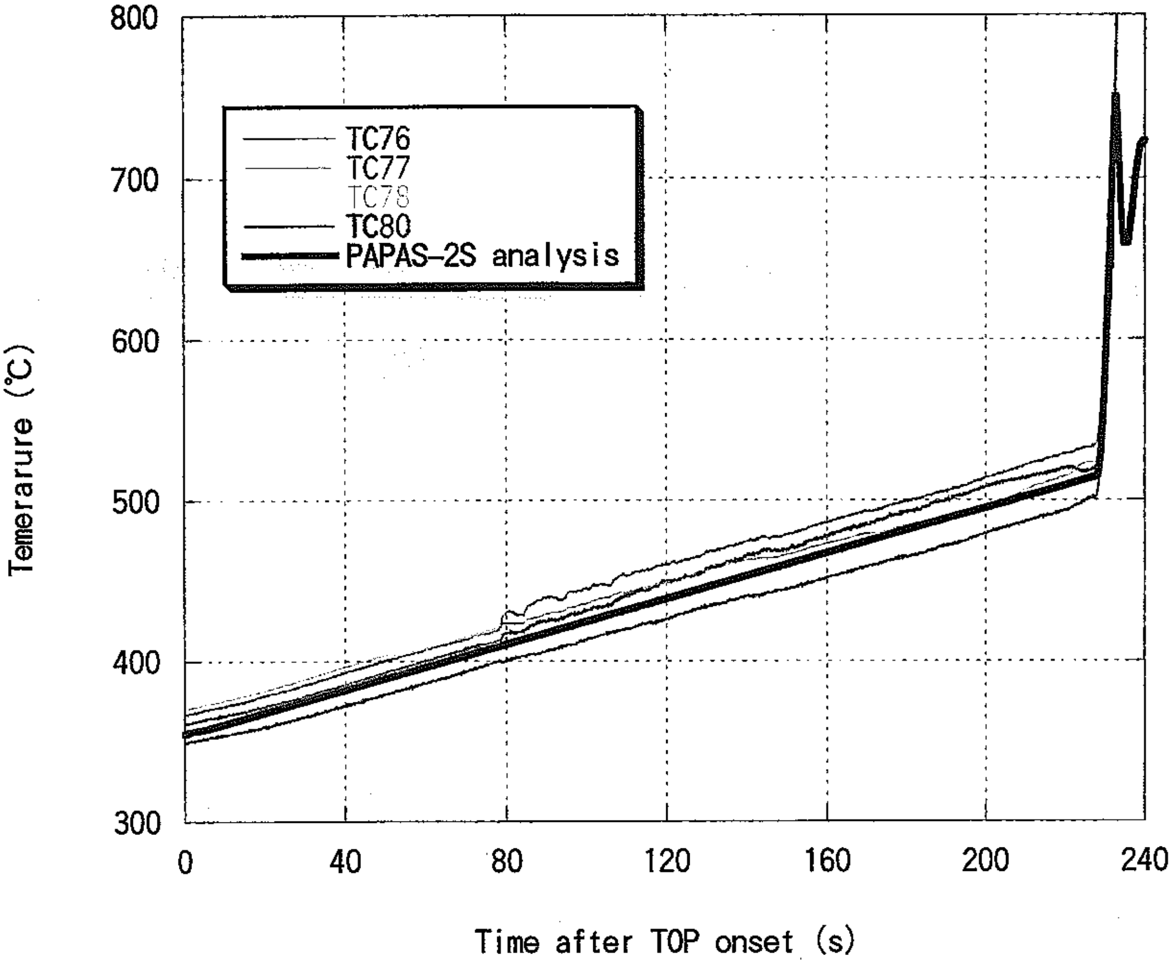

Figure 17 Comparison of coolant temperature history at TFC in the RB2 test

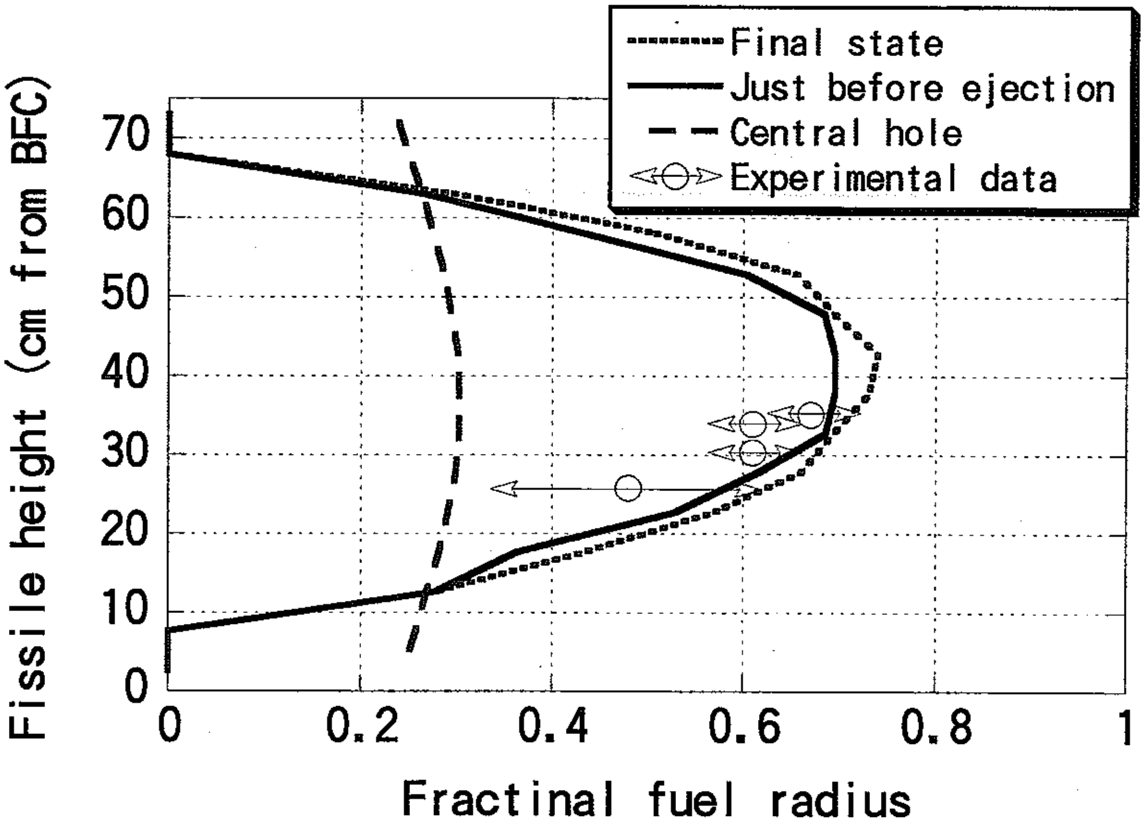

Figure 18 Comparison of fuel melting boundary in the RB2 test

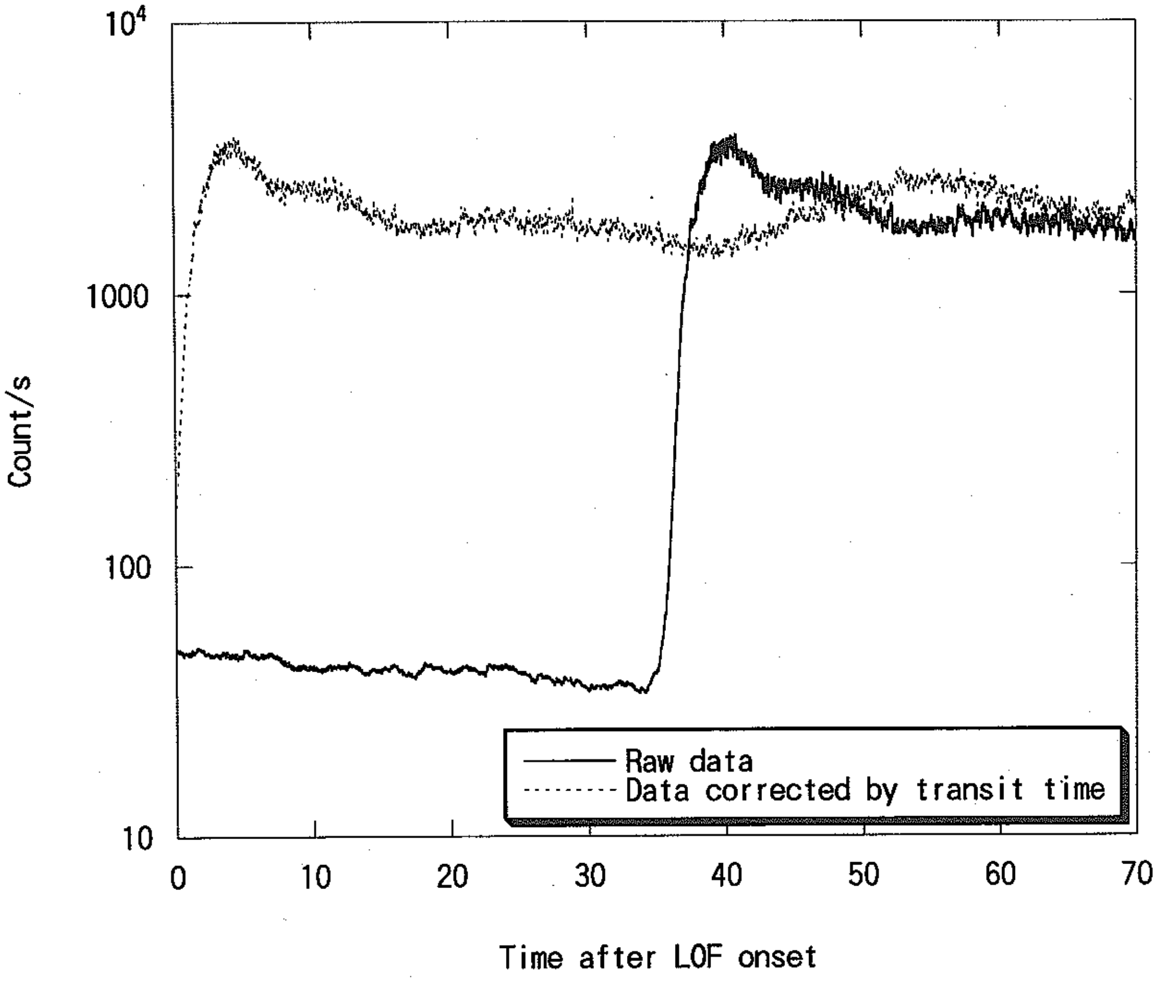

Figure 19 DN signal in the RB1 test

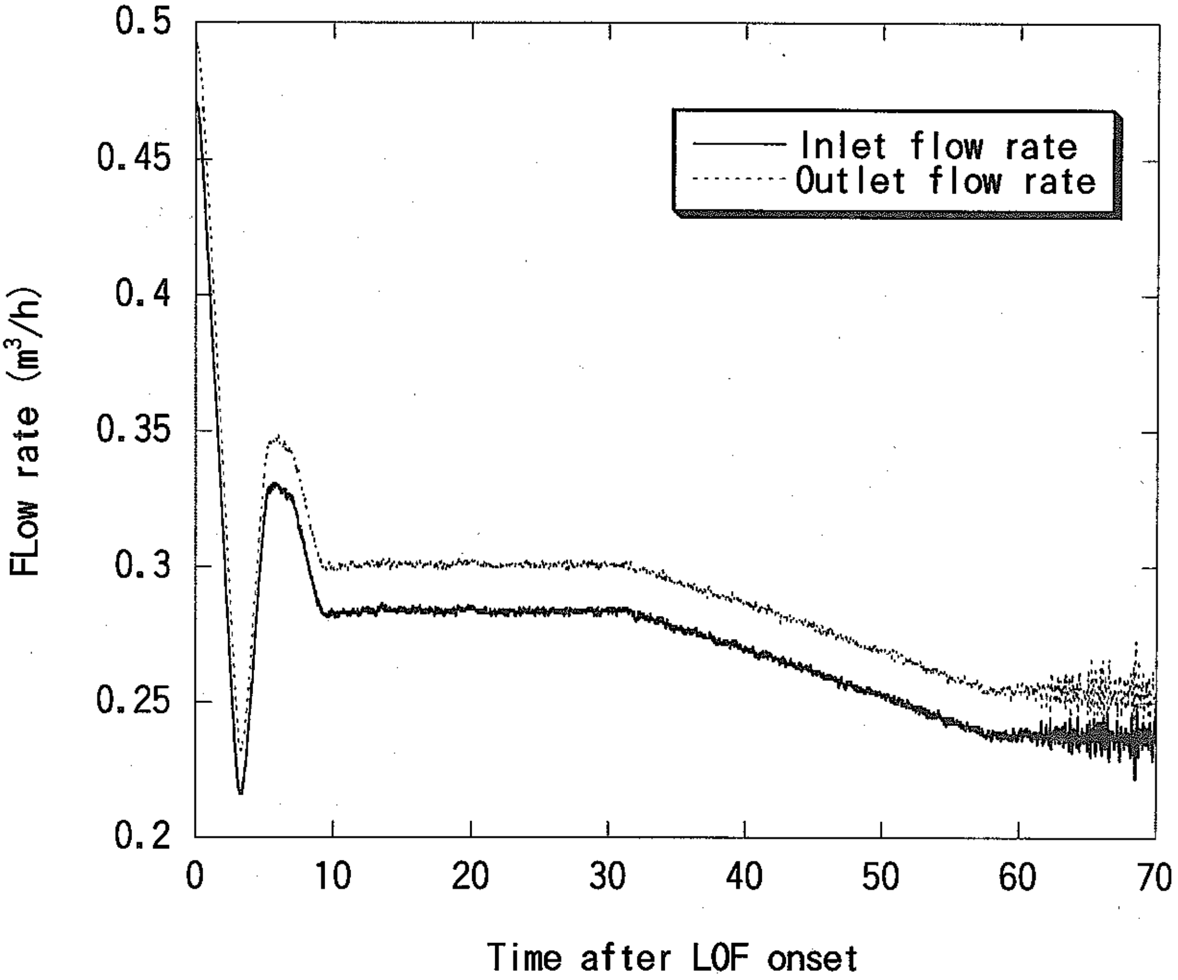

Figure 20 Inlet and outlet flow history in the RB1 test

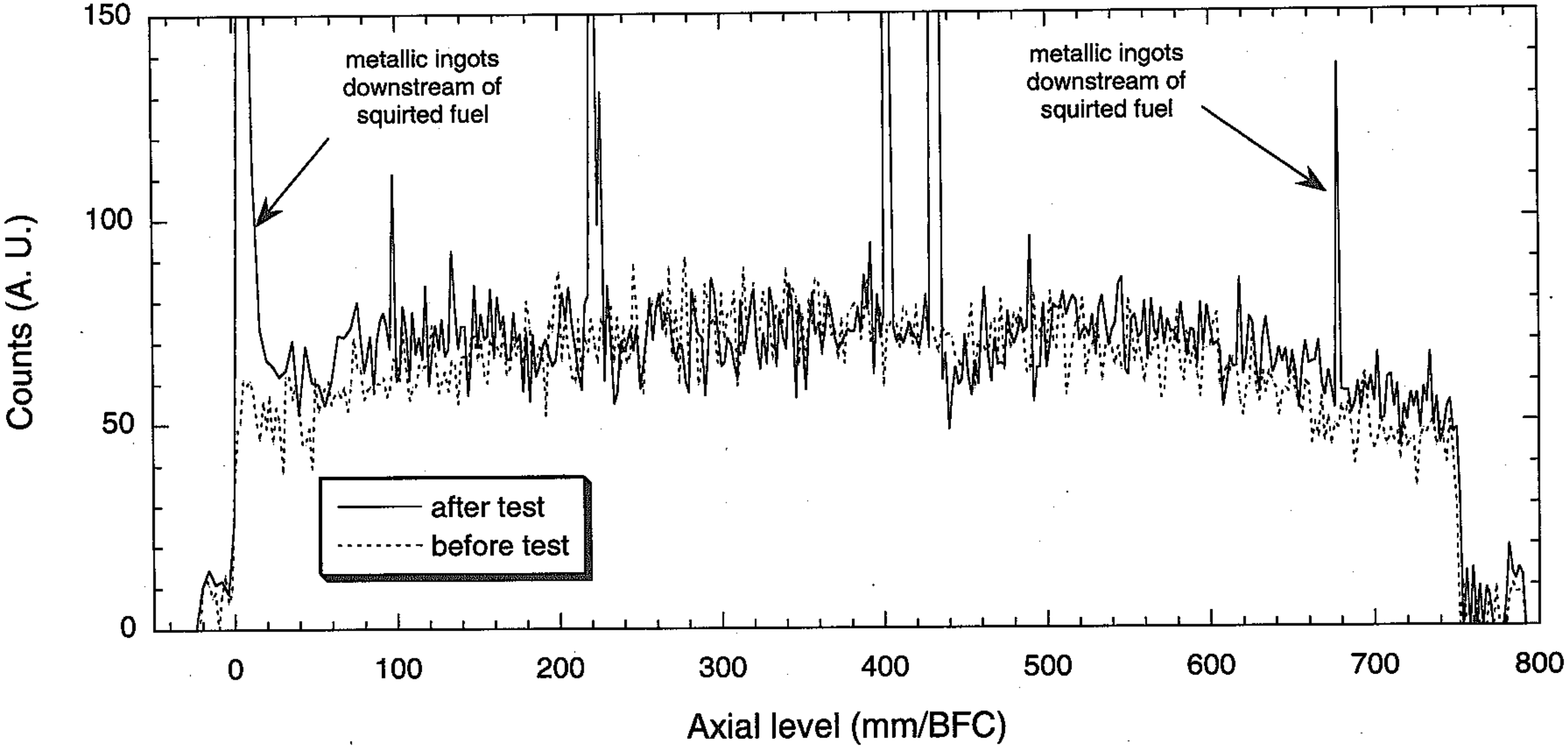

Figure 21 ^{106}Ru axial profile before and after the RB1 test

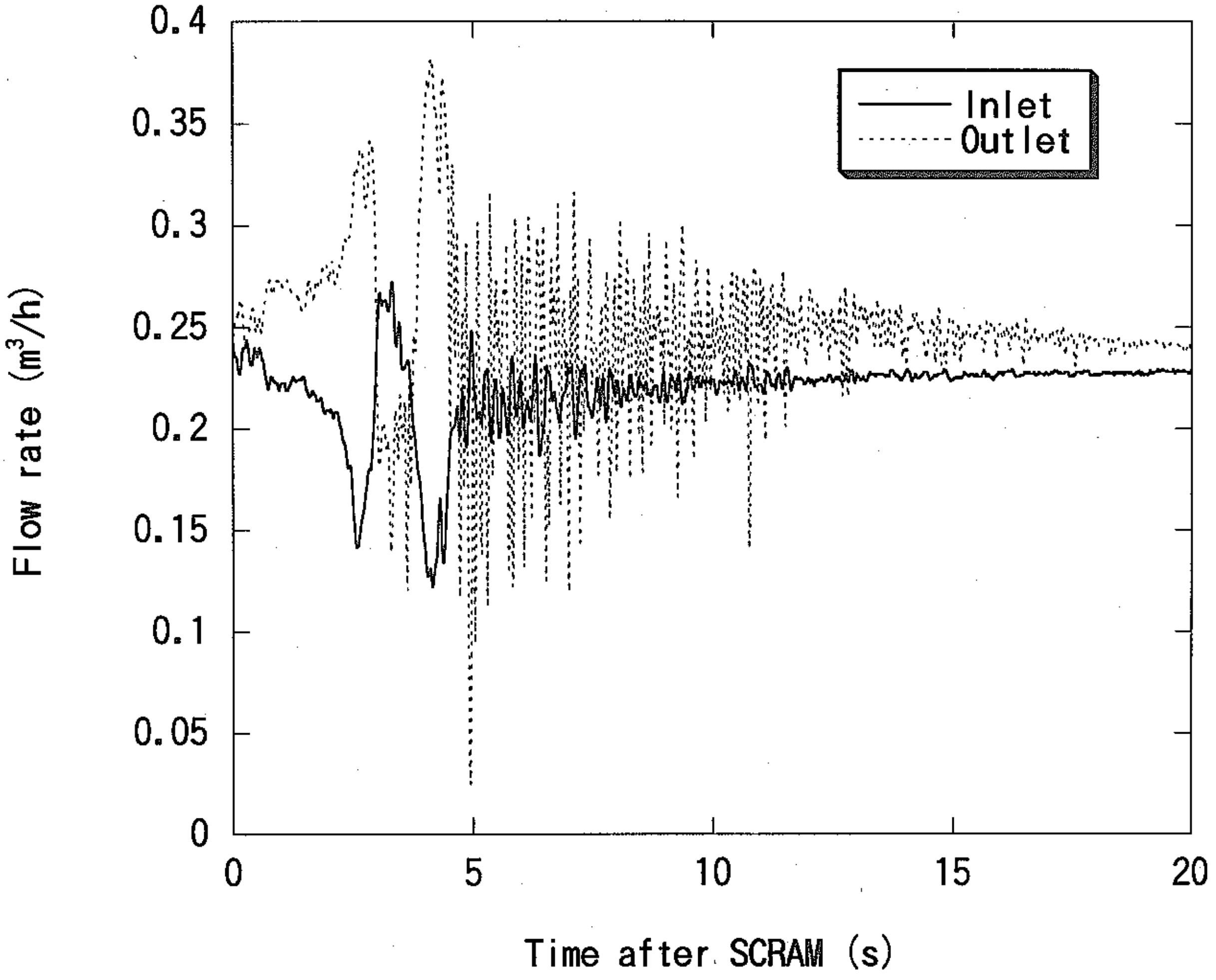

Figure 22 Inlet and outlet flow history after the SCARM in the RB1 test

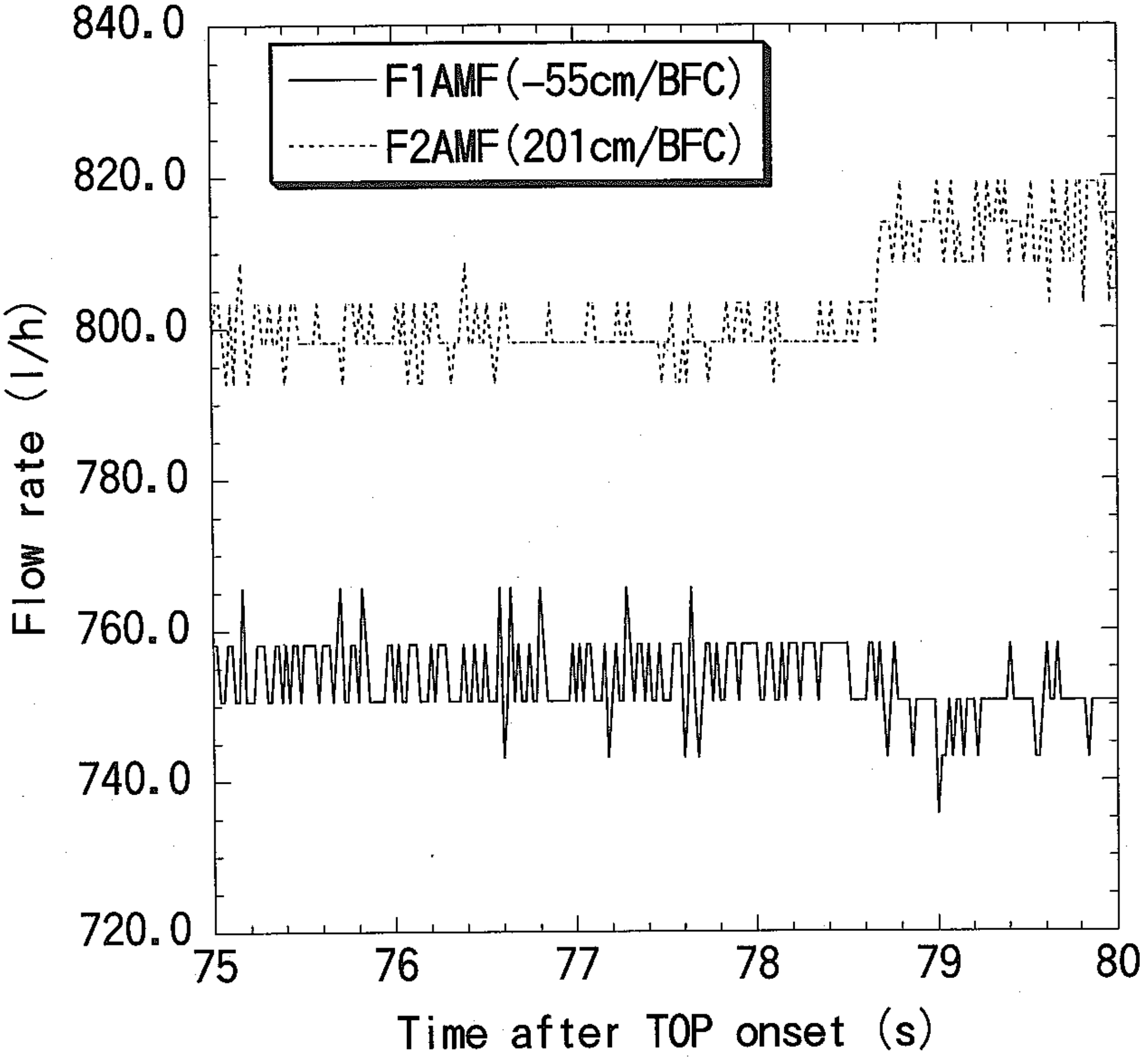

Figure 23 Inlet and outlet flow history durign the power ramp in the RB2 test

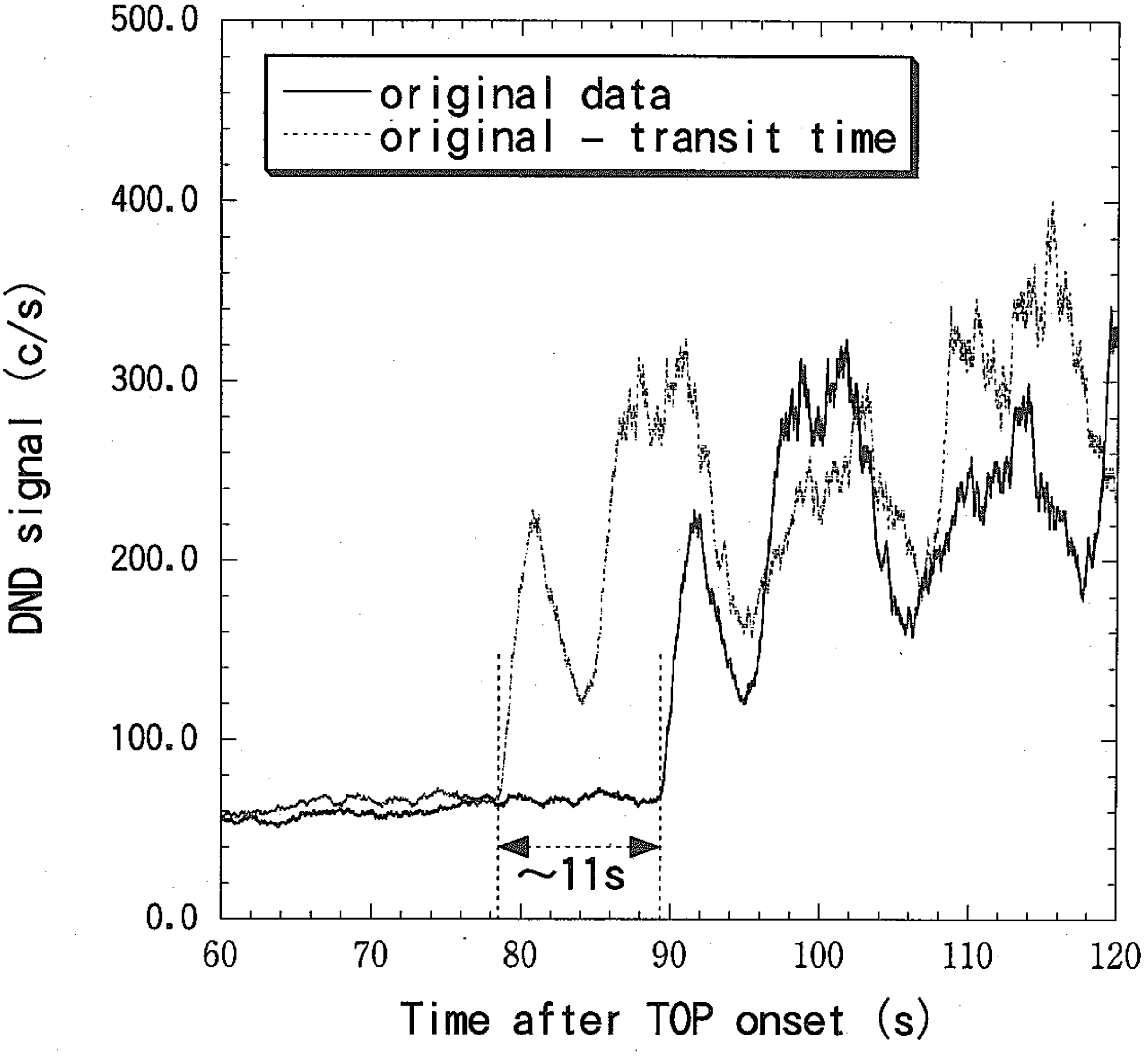

Figure 24 DN signal in the RB2 test

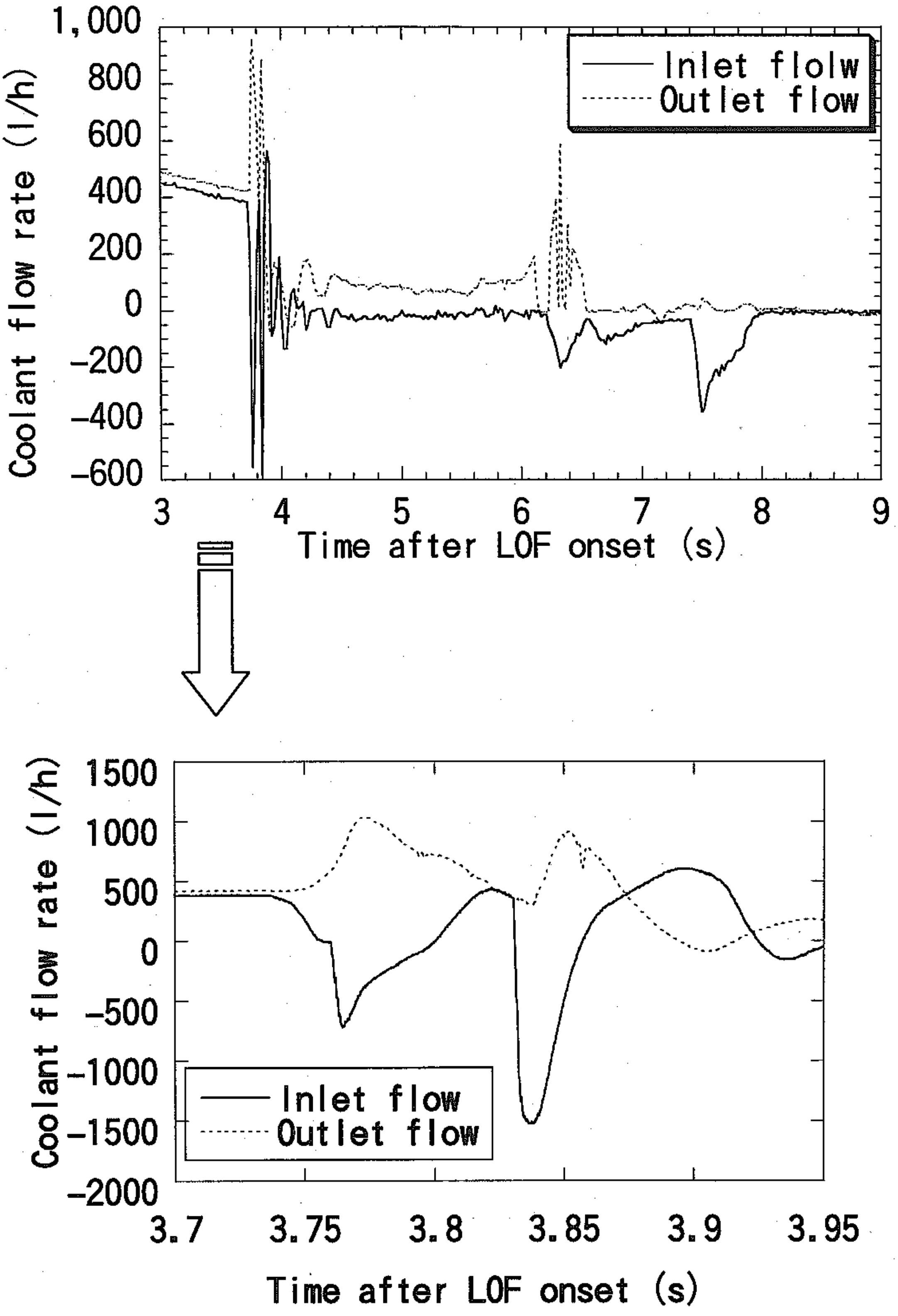

Figure 25 Inlet and outlet flow history during LOF in the RB2 test

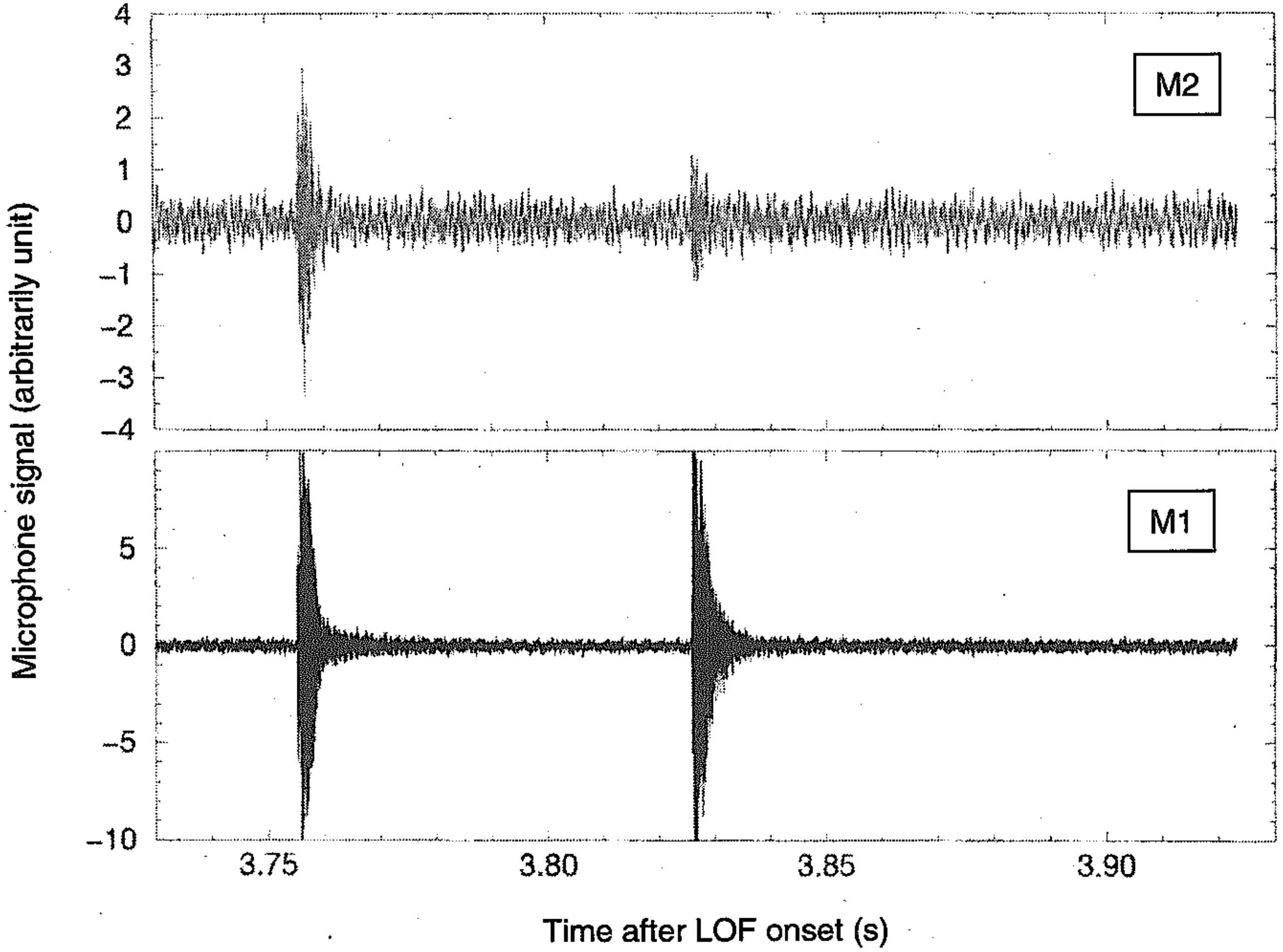

Figure 26 Microphone signal in the RB2 test

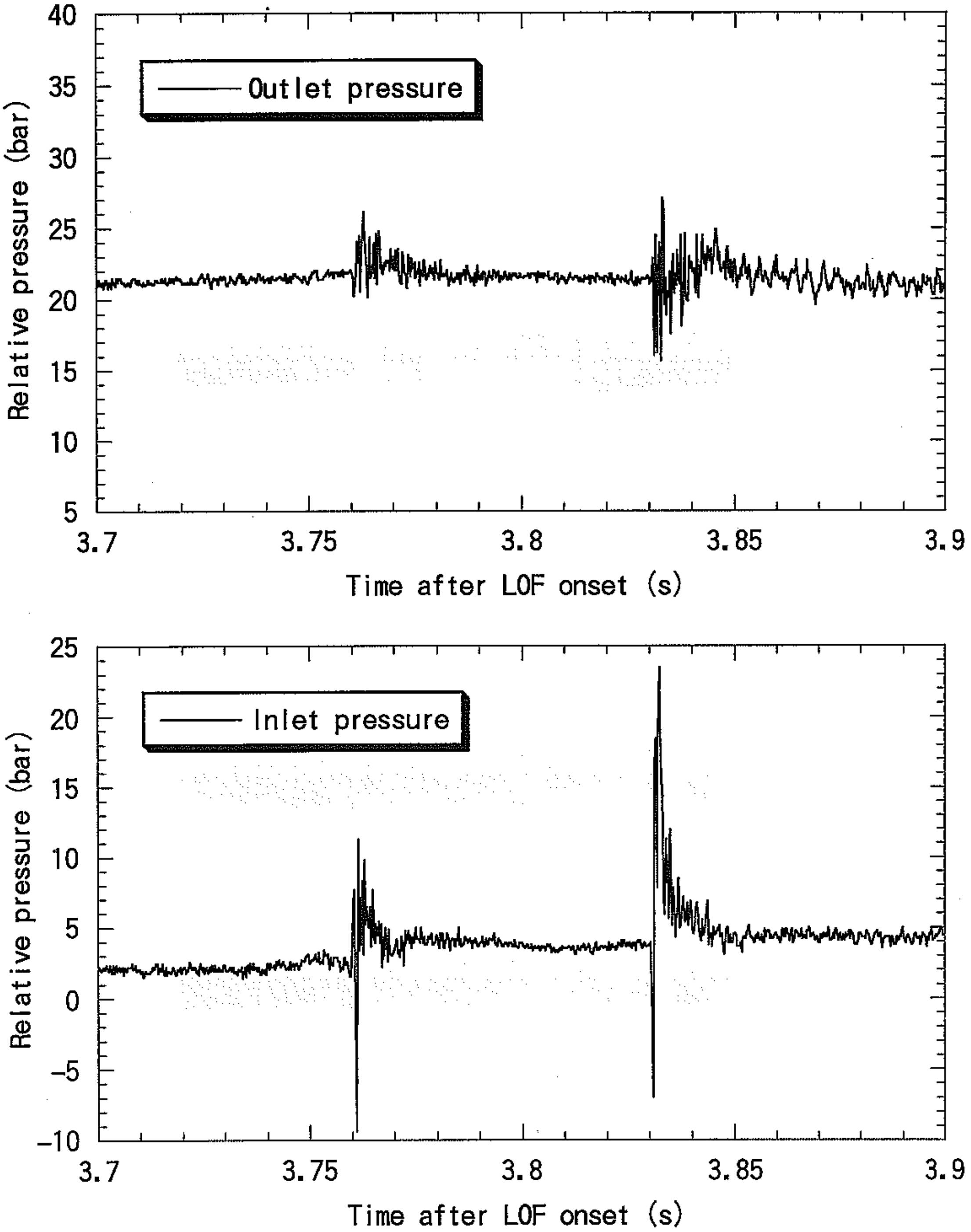

Figure 27 Inlet and outlet pressure in the RB2 test

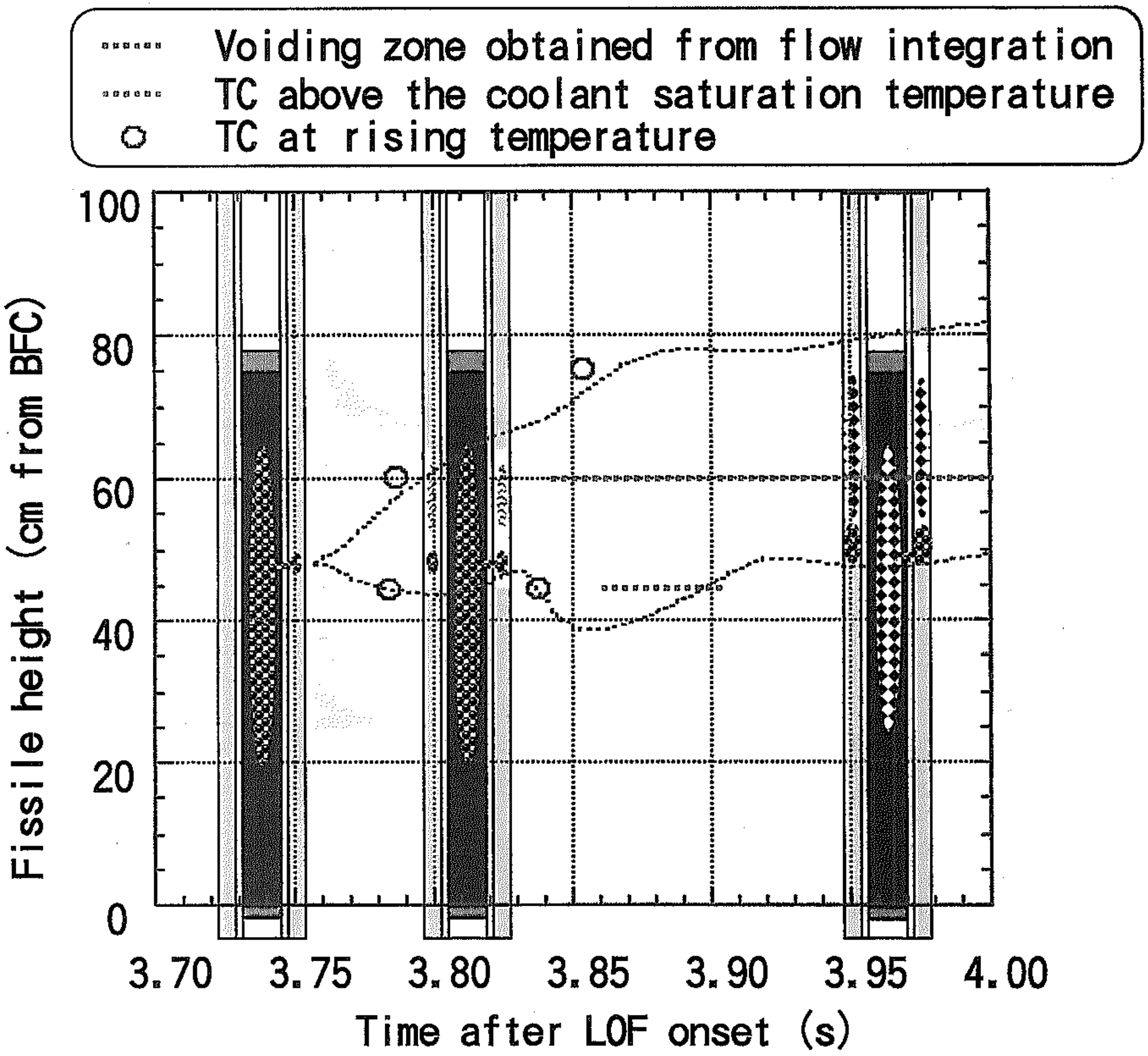

Figure 28 Voiding zone extension
after the molten fuel ejection in the RB2 test

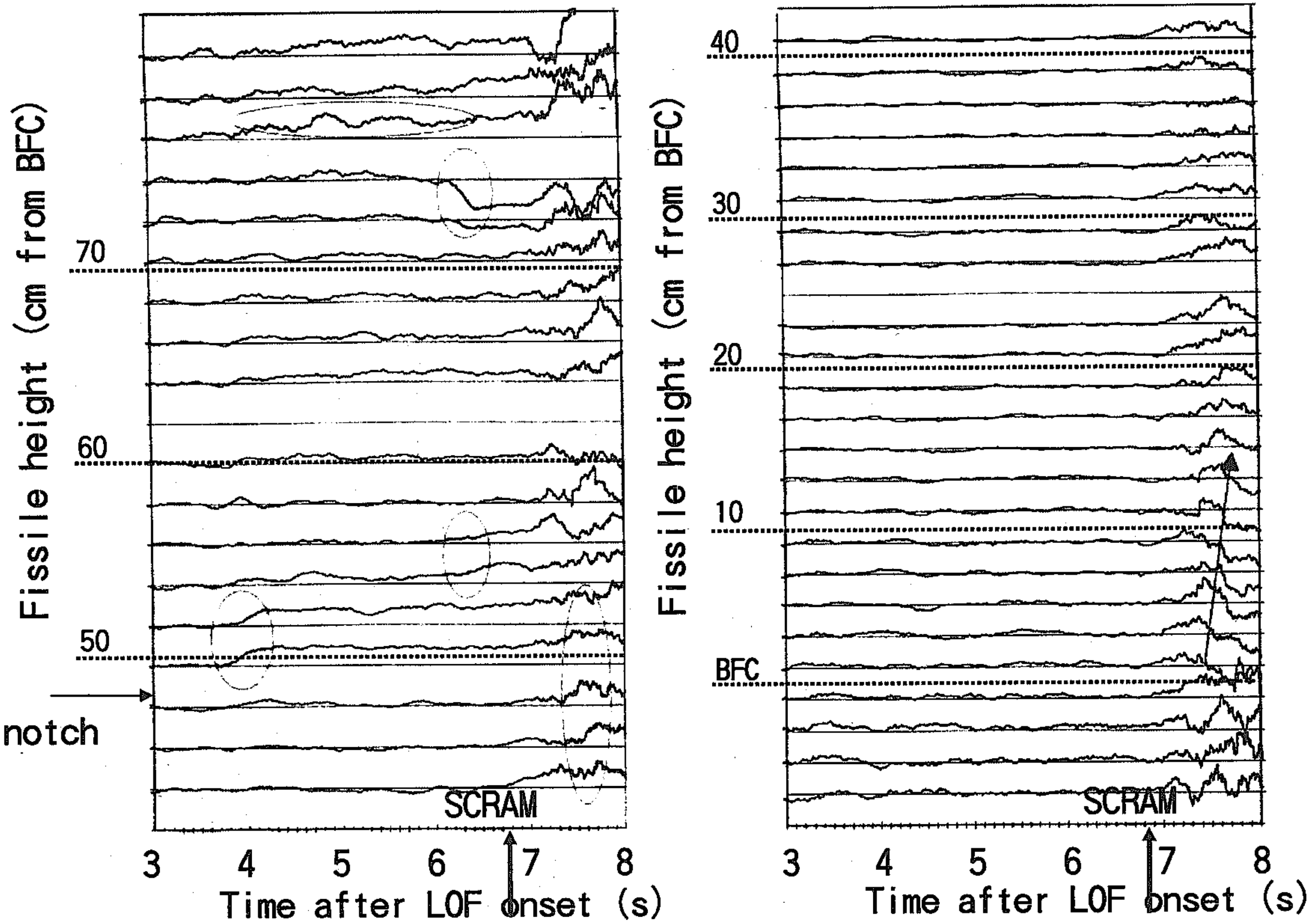

Figure 29 Neutron hodoscope data during LOF in the RB2 test

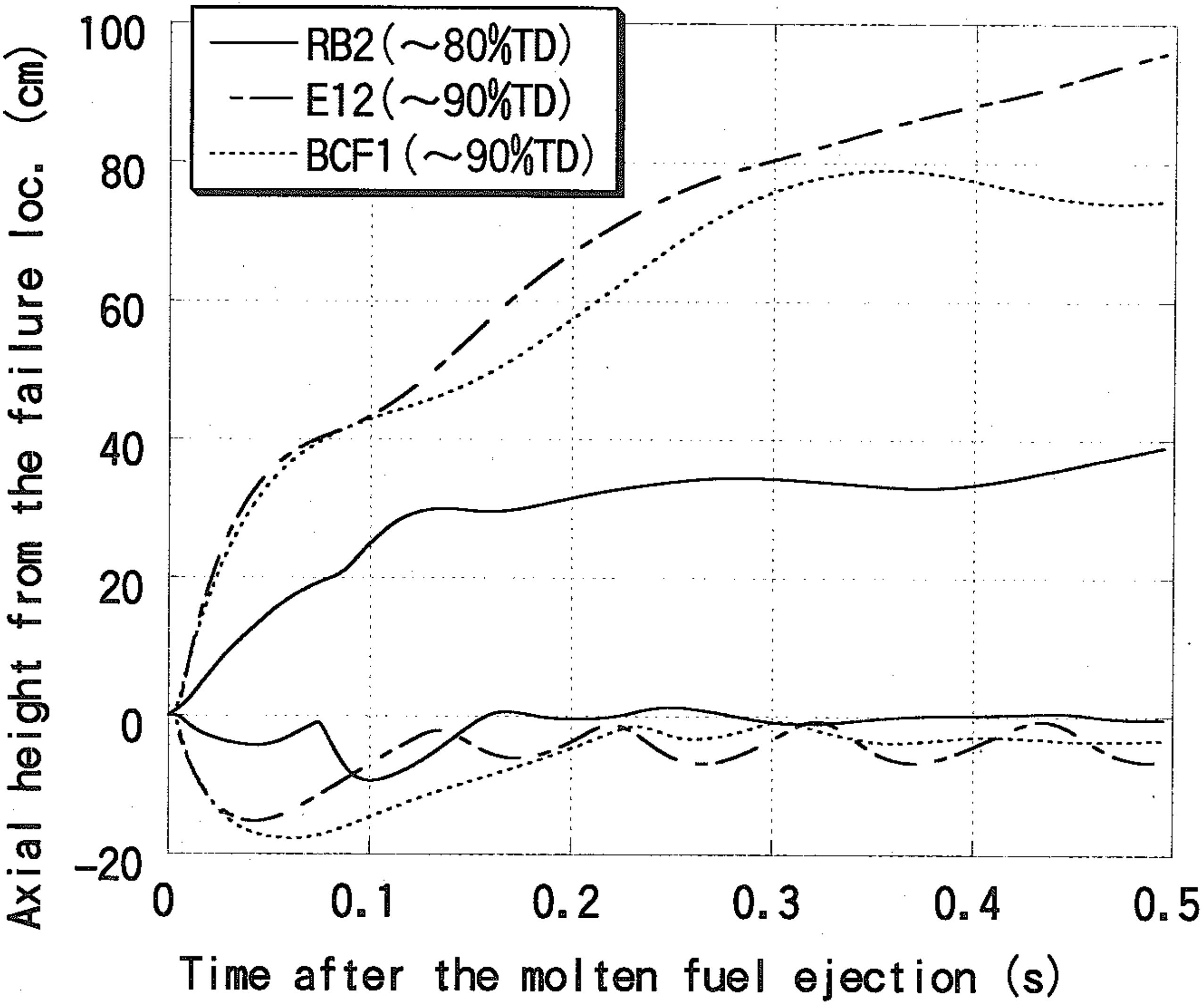

Figure 30 Comparison of RB2 voiding zone extension with the other CABRI tests

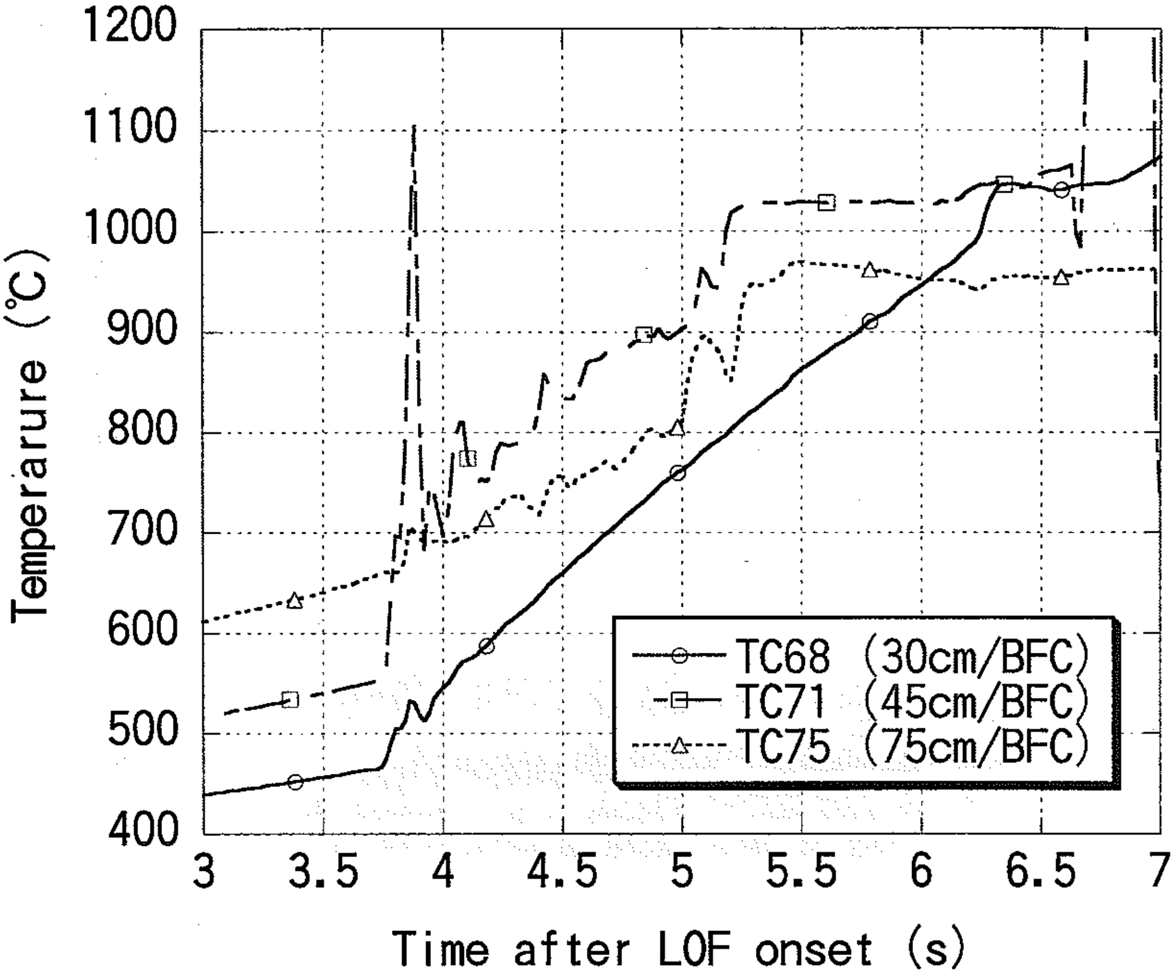

Figure 31 Coolant temperature history from 30 to 75 cm from BFC in the RB2 test

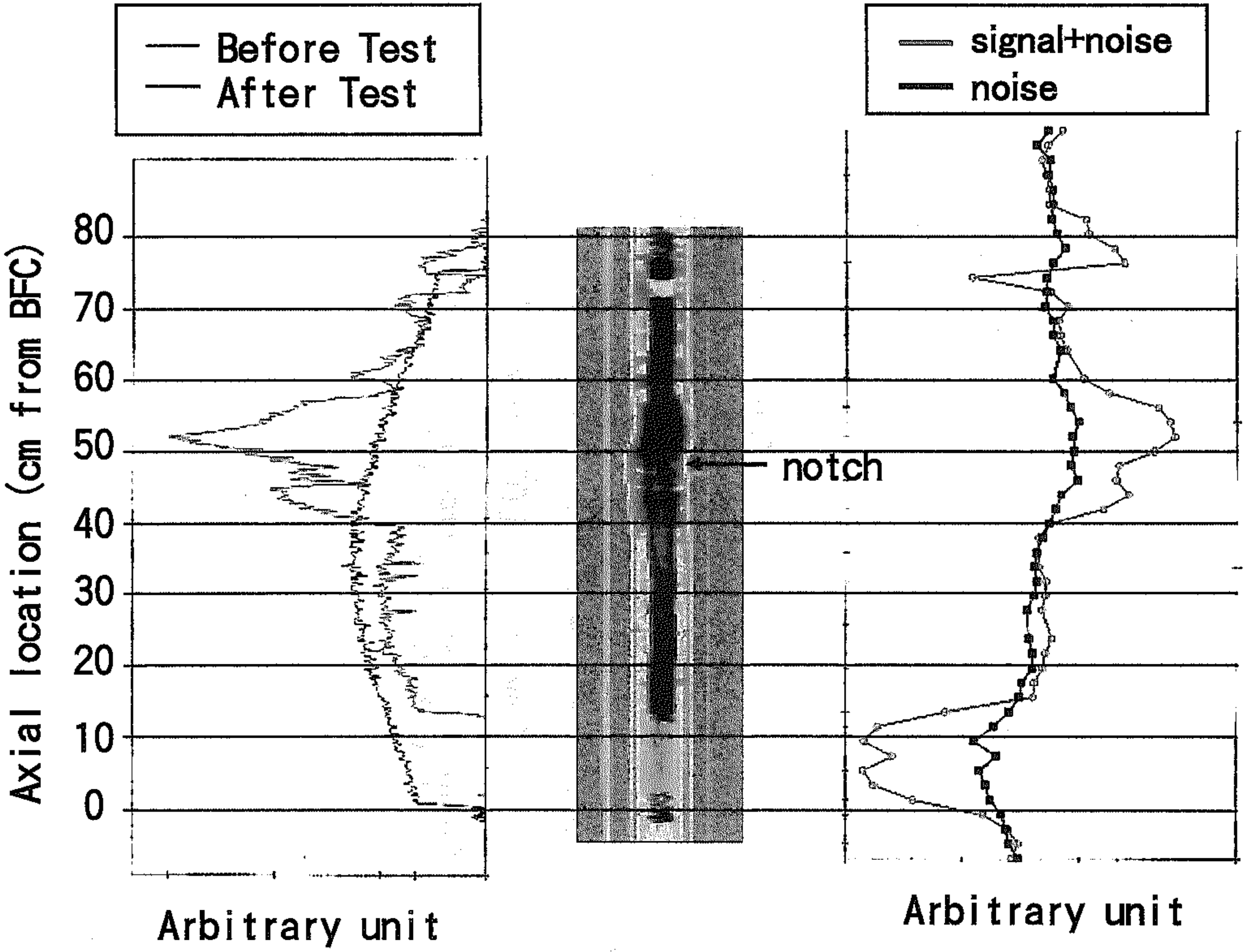

^{154}Eu γ scanning

X-ray radiography

Neutron hodoscope

Figure 32 Destructive and non-destructive PIE results in the RB2 test

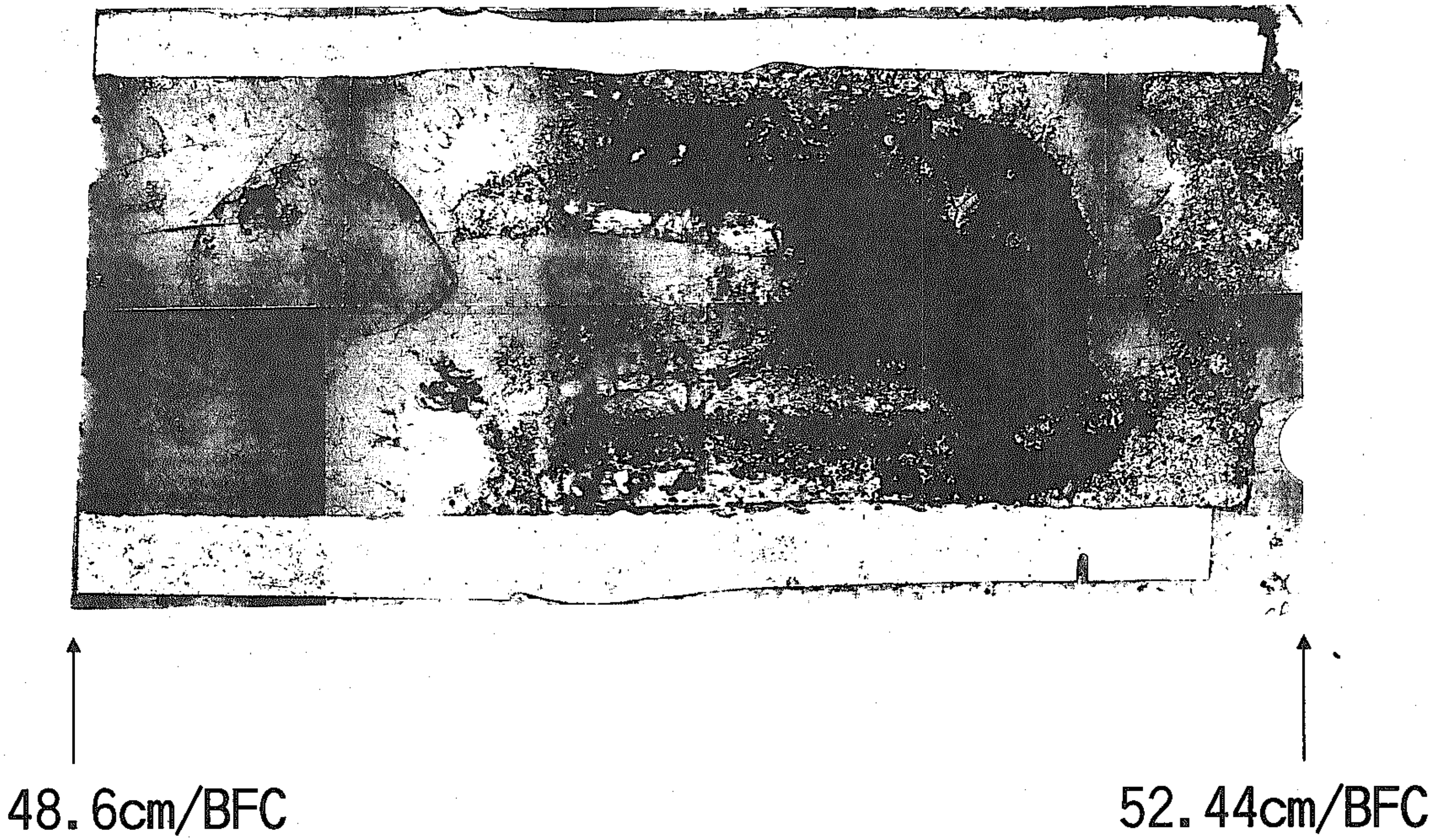

Figure 33 Axial cut of the RB2 test pin from 48.6 to 52.44 cm from BFC

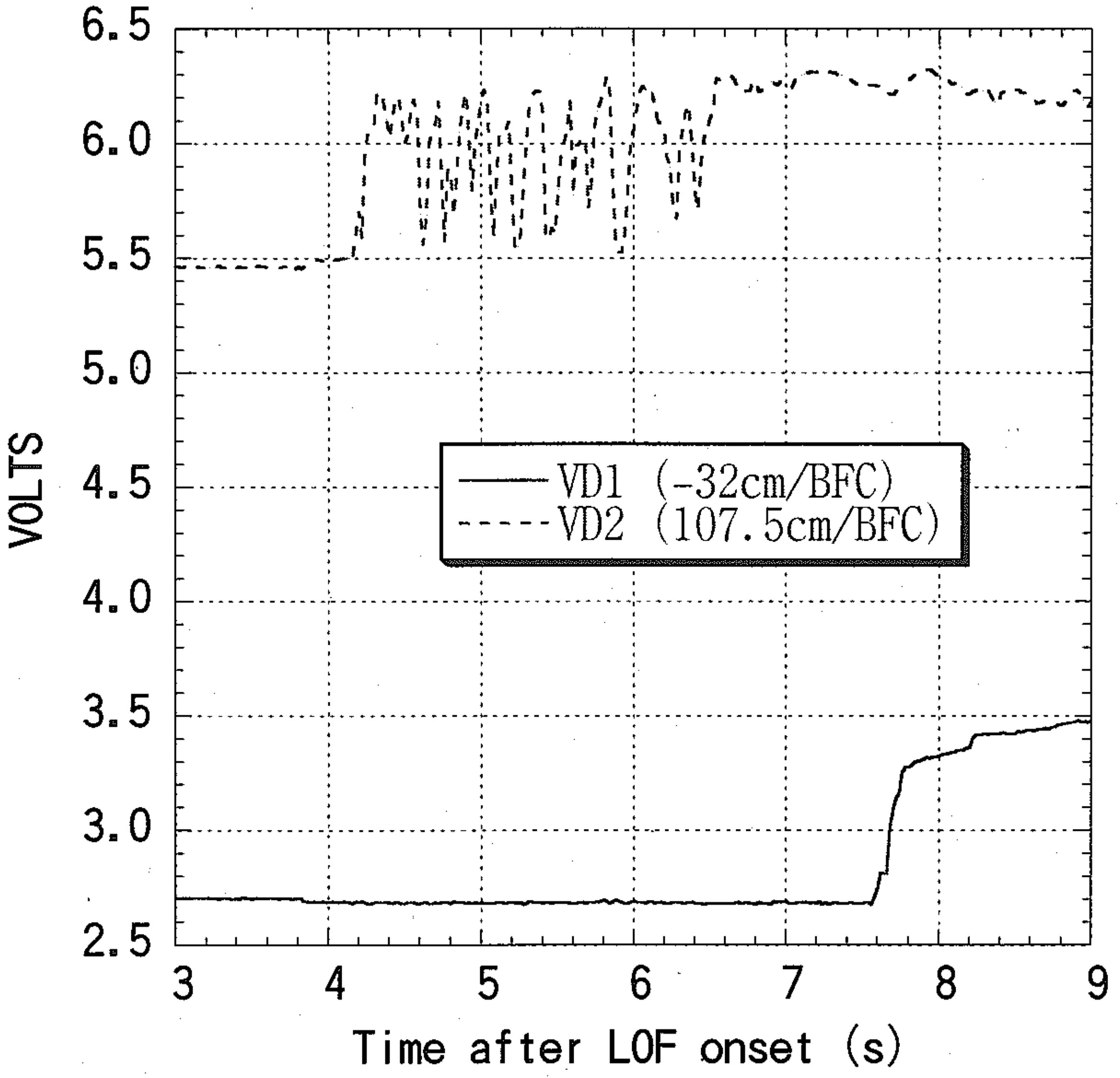

Figure 34 Void detector signal in the RB2 test

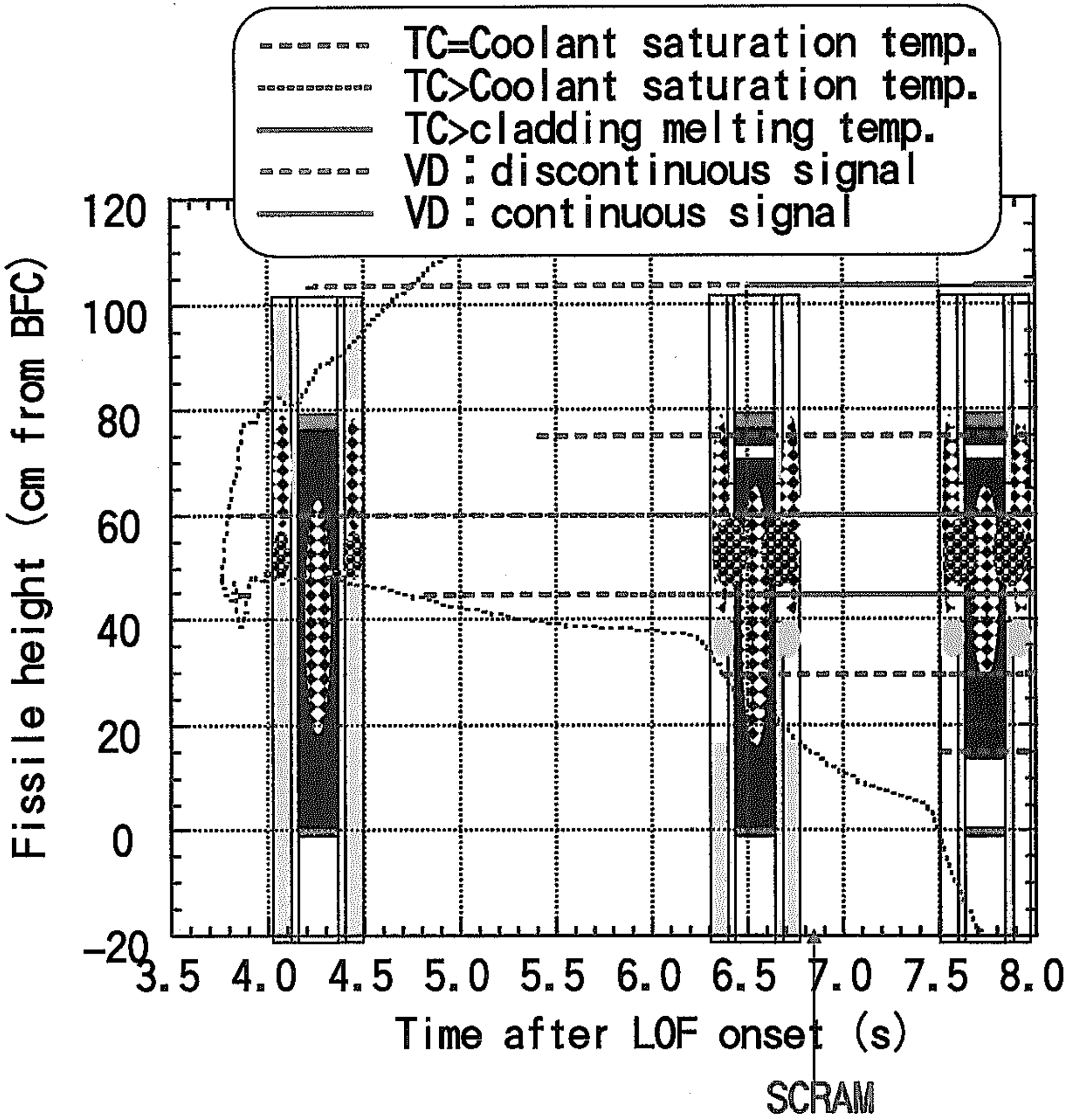

Figure 35 Fuel ejection and void development behavior in the RB2 test

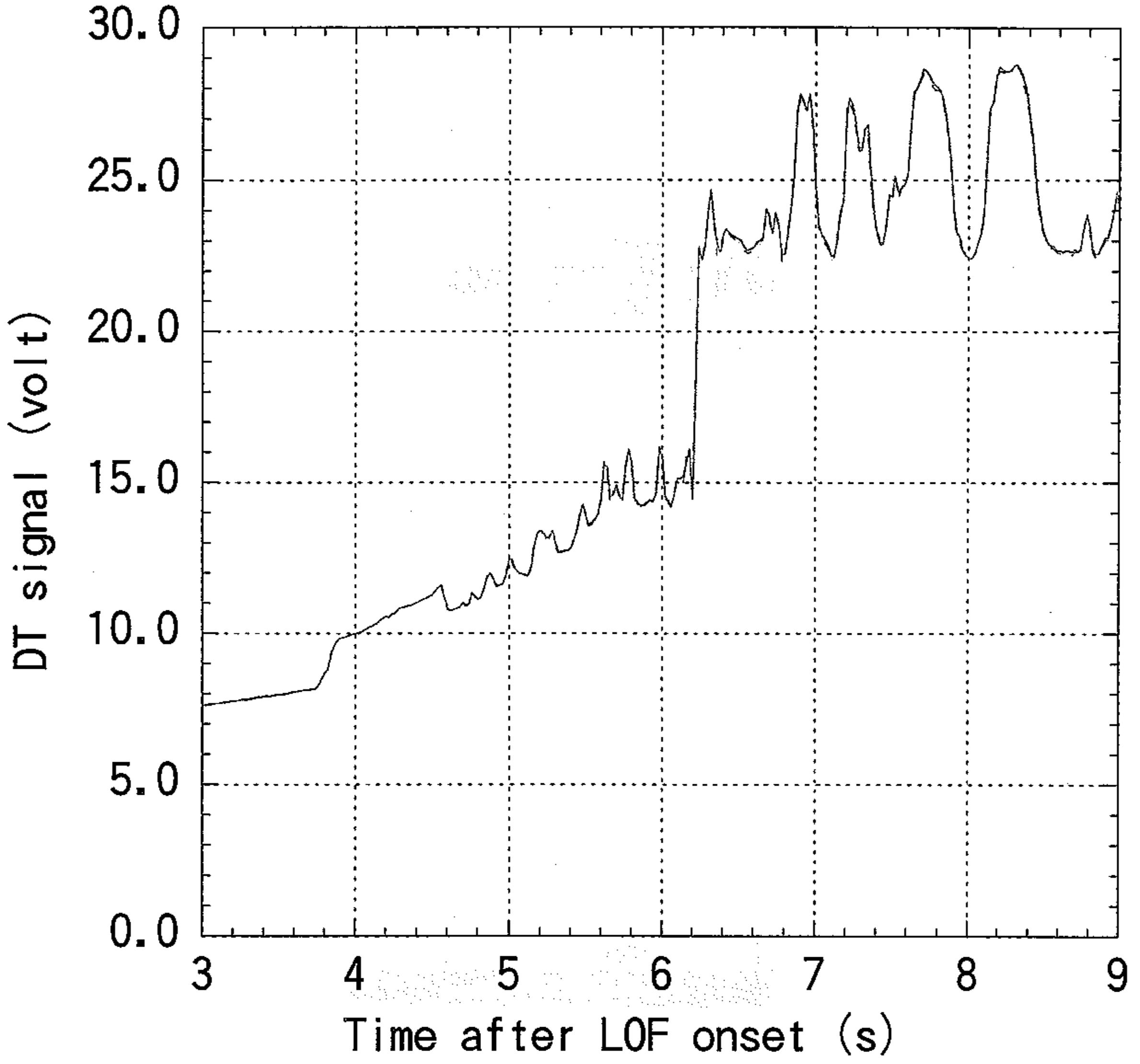

Figure 36 Displacement transducer signal in the RB2 test

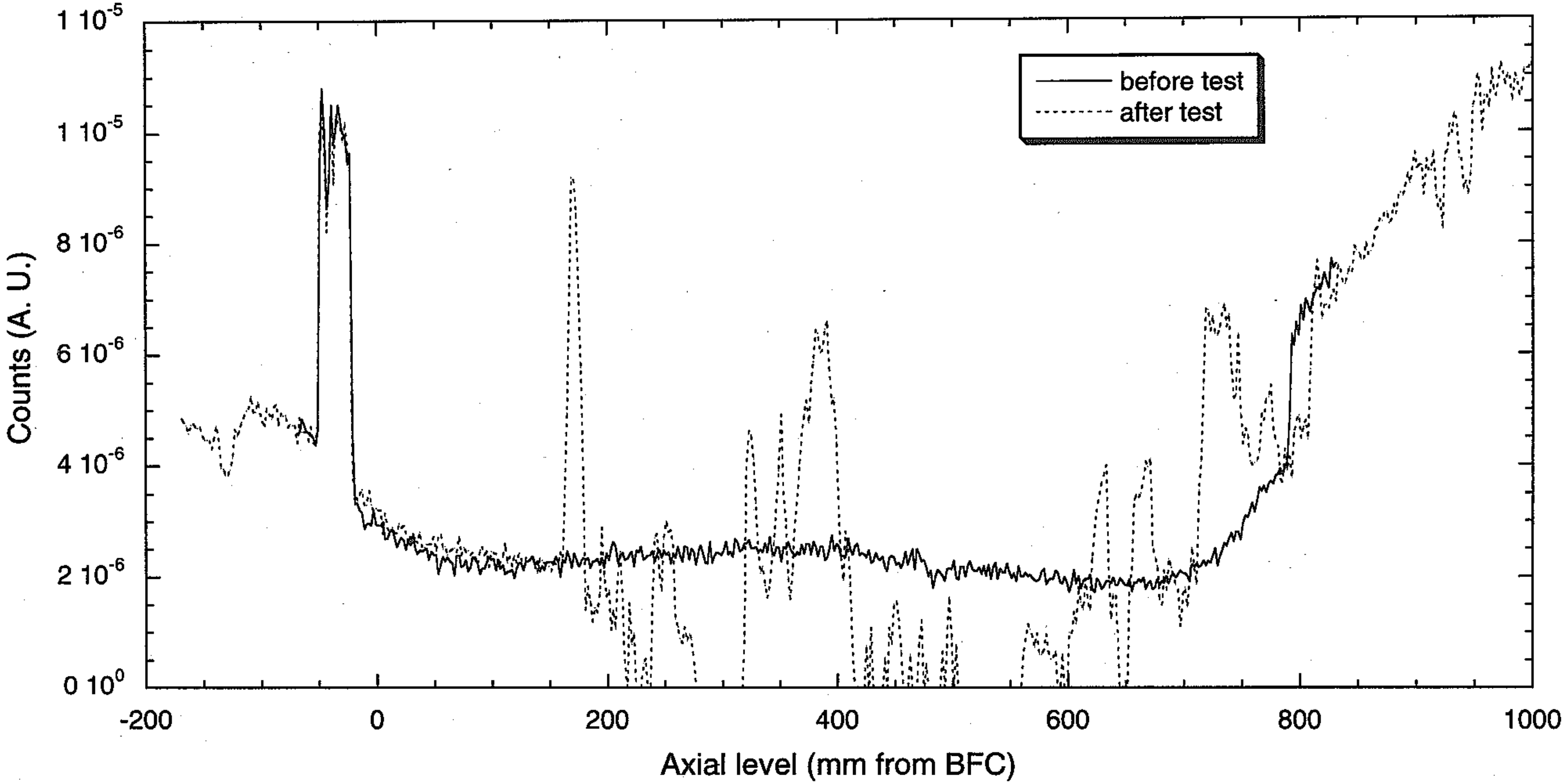

Figure 37 Axial profile of ^{60}Co gamma scanning in the RB2 test

Accumulation of the once molten steel

Figure 38 Radial cut of the RB2 test pin at 38.6 cm from BFC

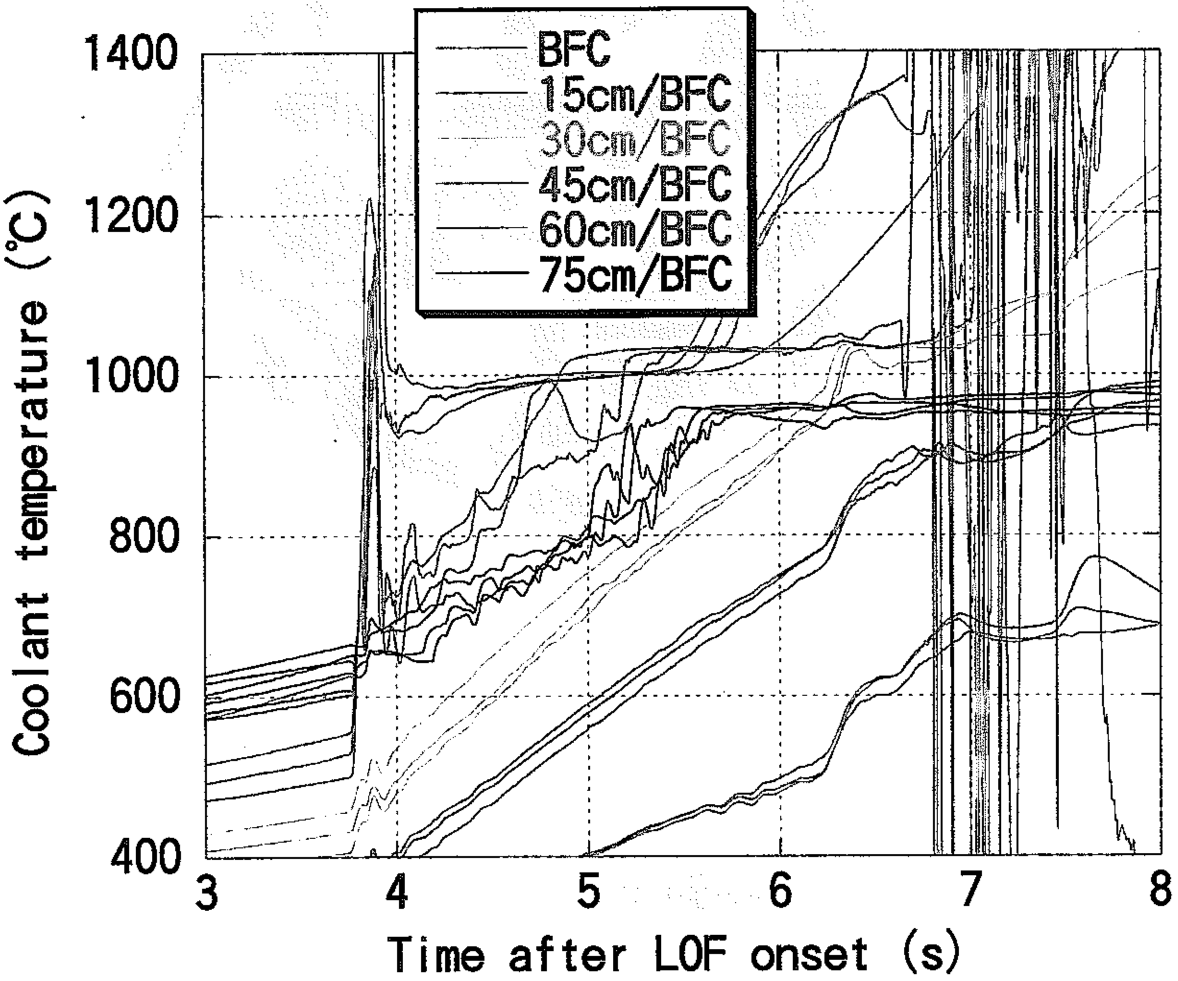

Figure 39 Coolant temperature history during the LOF in the RB2 test

	J1	R12
Fuel burn-up (at.%)	7	0
Mass of ejected fuel(g)	50	60
Flow recovery (%)	90	100

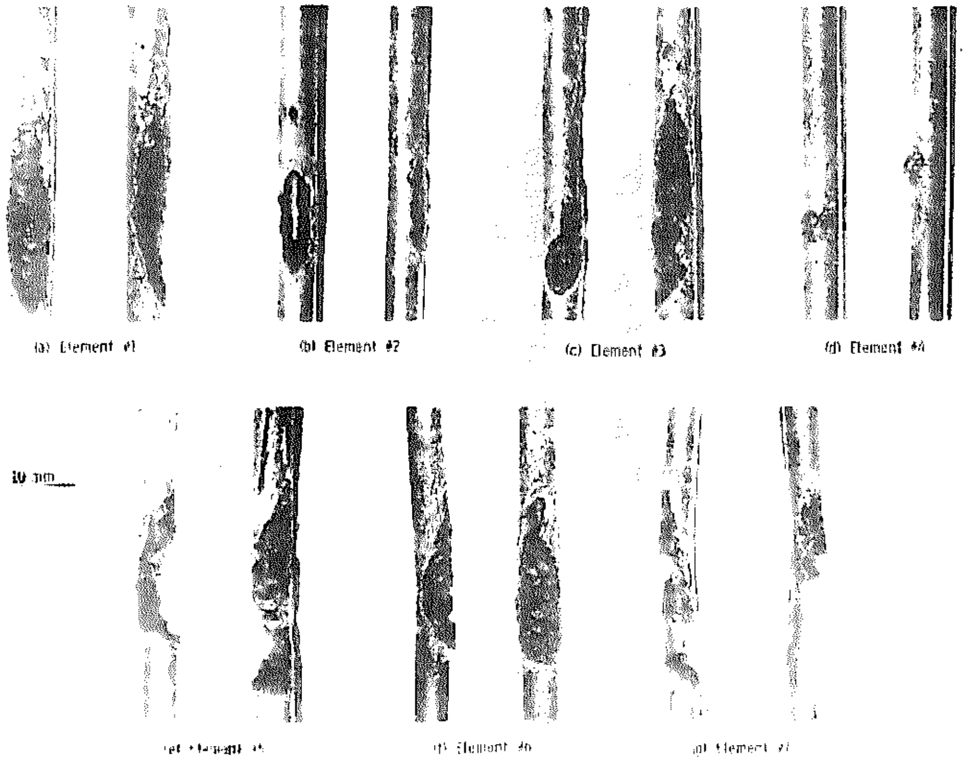

Fuel pins after the R12 test

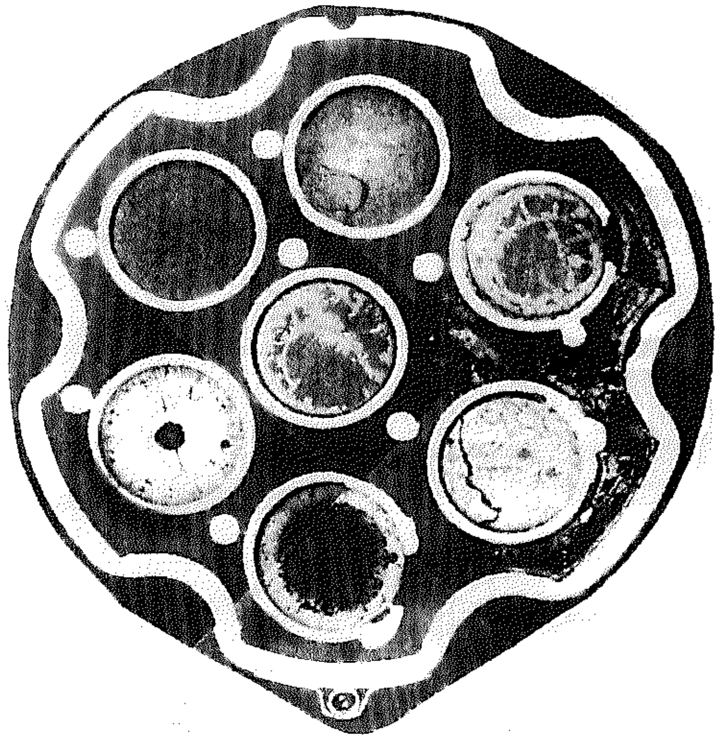

Radial cut in the J1 test (X/L=1.04)

Figure 40 Summary of the TREAT/J1 and R12 tests